

# **Twisted Intramolecular Charge transfer: Analysis through Spectrally Dispersed Impulsive Stimulated Raman Spectroscopy and TD-DFT calculations**

A dissertation submitted for the partial fulfillment of the requirements for the degree of

**BS-MS (Dual Degree)**

in

CHEMICAL SCIENCES

by

**AJAY JAYACHANDRAN (MS16057)**

at

**INDIAN INSTITUTE OF SCIENCE EDUCATION AND RESEARCH MOHALI**



April 2021



# CERTIFICATE OF EXAMINATION

This is to certify that the dissertation titled “**Twisted Intramolecular Charge transfer: Analysis through Spectrally Dispersed Impulsive Stimulated Raman Spectroscopy and TD-DFT calculations**” submitted by **Mr. Ajay Jayachandran** (Reg. No. MS16057) for the partial fulfilment of BS-MS dual degree programme of the Institute, has been examined by the thesis committee duly appointed by the Institute. The committee finds the work done by the candidate satisfactory and recommends that the report be accepted.

Dr.KR Shamasundar

Dr.Sanchita Sengupta

Dr. Arijit Kumar De  
(Supervisor)

**Date:** April 08, 2021



# DECLARATION

The work presented in this dissertation has been carried out by me under the guidance of Dr. Arijit Kumar De at the Indian Institute of Science Education and Research Mohali.

This work has not been submitted in part or in full for a degree, a diploma, or a fellowship to any other university or institute. Whenever contributions of others are involved, every effort is made to indicate this clearly, with due acknowledgement of collaborative research and discussions. This thesis is a bonafide record of original work done by me and all sources listed within have been detailed in the bibliography.

Ajay Jayachandran

(Candidate)

**Date:** April 08, 2021

In my capacity as the supervisor of the candidate's project work, I certify that the above statements by the candidate are true to the best of my knowledge.

Dr. Arijit Kumar De

(Supervisor)

# ACKNOWLEDGEMENTS

First of all, I would like to thank Dr. Arijit Kumar De for providing me with interesting problems to work on and for the insightful discussions to solve them.

I would like to thank Dr.KR Shamasundar, Dr.Sanchita Sengupta for their valuable scientific comments which provided great help in the project.

I would also like to thank my lab members Dr. Arindam Das, Dr. Subhash Chander, Ms.Yogita Silori, Dr. Anita Devi , Ms. Shaina Dhamija, Mr. Sumit Yadav , Mr. Subho Mitra, Ms. Garima Bhutani, Ms. Sakshi Chawla, Dr. Anita Yadav , Ms. Shradha Sapru and Ms. Umang Gupta for their constant support, inspiration and fruitful discussions.

I would like to thank IISER Mohali for all the instrumentation facilities and the library for providing access to a plethora of journals.

And finally, to my friends and family for their constant motivation and support.

# LIST OF FIGURES

Figure.1.1: a) Schematic diagrams of the  $^1\text{LE}$  (blue),  $^1\text{ET}$  (green) and  $^1\text{CT}$  (red) states when: (b)  $^1\text{LE}$  and  $^1\text{ET}$  character are comparable to each other, (c) when the steric restriction (black) is introduced to twist the D–A junction (e.g. an alkyl group at ortho-position) and (d) when the D–A junction is made coplanar

Figure 1.2: Photograph and emission spectra of DNS in solvents of increasing polarity. H, hexane; CH, cyclohexane; T, toluene; EA, ethyl acetate; Bu, n-butanol.

Figure 1.3: Jablonski diagram for fluorescence with solvent relaxation

Figure 1.4: Fluorescence spectra of DMABN and the model compounds in  $\text{CH}_2\text{Cl}_2$  at 25°C

Figure 2.1: Schematic of a pump – probe experiment

Figure 2.2: Types of signals in a pump – probe experiment

Figure 2.3: Energy level diagram showing the pulse sequence in ISRS involving electric field interactions from Raman pump and probe

Figure 2.4: Energy level diagrams showing the pulse sequence in resonant ISRS corresponding to each electronic transient (top) followed by double sided Feynman diagram that shows the phase matching condition for each of the third order Liouville pathways

Figure 2.5: Energy level diagram for TR-ISRS experiment

Figure 3.1: The experimental set-up for non-resonant ISRS along with a scheme for obtaining Raman spectrum

Figure 3.2: a) Absorption spectra of Nile blue (blue, solid line), Raman pump spectrum (red, filled plot) along with Gaussian fit (red, solid line) and WL probe spectrum (black, solid line)  
b) Molecular structure of Nile blue

Figure 3.3: Time-domain data (blue curve) at ~625 nm (GSB) recorded for Nile blue, polynomial fit to the data (red, solid line) (b) Processed data (blue curve) (c) Fourier transform of processed data giving Raman spectrum showing  $594\text{ cm}^{-1}$  mode

Figure 3.4: Time-domain data (blue curve) at ~530 nm (ESA) recorded for Nile blue, polynomial fit to the data (red, solid line) (b) Processed data (blue curve) (c) Fourier transform of processed data giving Raman spectrum without any noticeable Raman peak

Figure 3.5: a) Absorption spectra of methylene blue (blue, solid line), Raman pump spectrum (red, filled plot) along with Gaussian fit (red, solid line) and WL probe spectrum (black, solid line) b) Molecular structure of methylene blue

Figure 3.6: Time-domain data (blue curve) at ~636 nm (GSB) recorded for methylene blue, polynomial fit to the data (red, solid line) (b) Processed data (blue curve) (c) Fourier transform of processed data giving Raman spectrum showing  $250\text{ cm}^{-1}$ ,  $361\text{ cm}^{-1}$  and  $534\text{ cm}^{-1}$  mode

Figure 3.7: Time-domain data (blue curve) at ~581 nm (ESA) recorded for methylene blue, polynomial fit to the data (red, solid line) inset. (b) Processed data (blue curve) (c) Fourier transform of processed data giving Raman spectrum showing  $250\text{ cm}^{-1}$  mode

Figure 3.8: Experimental set-up for TR- ISRS and data obtained for solvent (methanol)

Figure 3.9: Ground state geometry of a) methylene blue and b) Nile blue

Figure 3.10: Simulated Ground state vibrational modes represented by a) Raman Activity spectra b) Raman Intensity spectra c) Infrared Intensity Spectra for Nile blue in gaseous phase obtained at 6-31+g(d,p) basis set and B3LYP functional (unscaled)

Figure 3.11: Simulated Ground state vibrational modes represented by a) Raman Activity spectra b) Raman Intensity spectra c) Infrared Intensity Spectra for Nile blue in solvent phase (methanol) obtained at 6-31g+(d,p) basis set and B3LYP functional (unscaled)

Figure 3.12: Simulated UV/Visible Absorption spectra for Nile blue obtained at 6-311g++(d,p) basis set and M05-2X functional at solvent phase (Maximum intensity at 625 nm)



Figure 3.13: Simulated IR active vibrational modes of a) ground state spectra b) excited state spectra for Nile blue in solvent phase (methanol) obtained at 6-31g+(d,p) basis set and B3LYP functional

Figure 3.14: Simulated Ground state vibrational modes represented by a) Raman Activity spectra b) Raman Intensity spectra c) Infrared Intensity Spectra for methylene blue in gaseous phase obtained at 6-311g++(d,p) basis set and M05-2X functional (unscaled)

Figure 3.15: Simulated Ground state vibrational modes represented by a) Raman Activity spectra b) Raman Intensity spectra c) Infrared Intensity Spectra for methylene blue in solvent phase (methanol) obtained at 6-311g++(d,p) basis set and M05-2X functional (unscaled)

Figure 3.16: Simulated UV/Visible Absorption spectra for methylene blue obtained at 6-311g++(d,p) basis set and M05-2X functional at solvent phase (Maximum intensity at 580 nm)

Figure 3.17: Simulated IR active vibrational modes of a) ground state spectra b) excited state spectra for methylene blue in solvent phase (methanol) obtained at 6-31g+(d,p) basis set and M05-2X functional

Figure 4.1: Simulated Ground state vibrational modes represented by Raman Activity spectra for DMABN in solvent phase (methanol) obtained at 6-31g+(d,p) basis set and wB97XD functional (unscaled)

Figure 4.2: MO diagrams (isovalue 0.03) showing the flow of charge during vertical excitation and TICT formation a) HOMO b) LUMO of  $S_0$  planar geometry c) HOMO\* d) LUMO\* of  $S_1$  twisted geometry in DMABN, all obtained at 6-31g+(d,p) basis set and wB97XD functional in methanol solution IEFPCM model

Figure 4.3: Simulated IR active vibrational modes of a) ground state spectra b) excited state spectra for DMABN in solvent phase (methanol) obtained at 6-31g+(d,p) basis set and wB97XD functional (unscaled)

Figure 4.4: Constrained DFT/TDDFT optimization scans of the twist (rotation of C3-C4-N11- C12 dihedral) on  $S_0$  and  $S_1$  excited state surfaces for DMABN in solvent phase (methanol) obtained at 6-31g+(d,p) basis set and wB97XD functional

Figure 4.5: MO diagrams (isovalue 0.03) showing the flow of charge during vertical excitation and TICT formation a) HOMO b) LUMO of  $S_0$  planar geometry c) HOMO\* d) LUMO\* of  $S_1$  twisted geometry in DMPNA, all obtained at 6-31g+(d,p) basis set and wB97XD functional in methanol solution IEFPCM model.

Figure 4.6: Ground state geometry of DNS optimized at MO6-2X functional and 6-31g+(d,p) basis set using a) IEFPCM solvation model for a methanol solvent b) Explicit solvation (ratio1:1) c) Explicit solvation (ratio2:1)

Figure 4.7: Simulated Raman active ground state vibrational modes obtained at a) explicit solvation model b) implicit solvation model for DNS in solvent phase (methanol) obtained at 6-31g+(d,p) basis set and MO6-2X functional (unscaled)

Figure 4.8: Van der Waals spheres in ground state obtained at a) explicit solvation model in 1:1 ratio b) explicit solvation model in 1:2 ratio of DNS and methanol using 6-31g+(d,p) basis set and MO6-2X functional. [Red arrow indicates position of methanol solvent molecule]

Figure 4.9: 2-D axis DNS with projection along  $C_{10}$ - $C_{25}$ - $C_{13}$ - $C_{15}$  dihedral coordinate represented in orthogonal planes, indicating the isomerisation pathway and charge transfer pathway

Figure 4.10: Optimised ground state geometry of a) cis-stilbene b) trans-stilbene obtained at 6-31g+(d,p) basis set and MO6-2X functional in methanol dielectric

Figure 4.11: Simulated Raman active ground state vibrational modes obtained at a) implicit solvation model b) of a) cis-stilbene b) trans-stilbene in methanol obtained at 6-31g+(d,p) basis set and MO6-2X functional [Red-Ring breathing mode, Blue-Double bond twisting mode, Green- Benzene H in-plane-out-of-plane Antisymmetric Bending mode] (unscaled)

## LIST OF TABLES

Table 3.1: Characterization of ground state vibrational frequencies of nile blue

Table 3.2: Characterization of ground state vibrational frequencies of methylene blue

Table 4.1 : Ground state geometry of DMABN optimized at wB97XD functional and 6-31g+(d,p) basis set using IEFPCM model of solvation containing a methanol dielectric

Table 4.2: Excited state geometry of DMABN optimized at wB97XD functional and 6-31g+(d,p) basis set using IEFPCM model of solvation containing a methanol dielectric

Table 4.3: Ground and Excited state vibrational frequency characterization

# ABBREVIATIONS

DFT	Density Functional Theory
DMABN	4-(N,N-dimethylamino)benzonitrile
DMPNA	N,N-dimethyl-p-nitroaniline
DNS	4-dimethylamino-4'-nitrostilbene
ESA	Excited State Absorption
FSRS	Femtosecond Stimulated Raman Spectroscopy
GSB	Ground State Bleach
ISRS	Impulsive Stimulated Raman Spectroscopy
MM	Molecular Mechanics
NOPA	Noncollinear Optical Parametric Amplifier
PES	Potential Energy Surface
QM	Quantum Mechanics
SE	Stimulated Emission
TAS	Transient Absorption Spectroscopy
TD-DFT	Time Dependent Density Functional Theory
TICT	Twisted Intermolecular charge transfer
TR-ISRS	Time Resolved Impulsive Stimulated Raman Spectroscopy
UV/IR	Ultra Violet / Infra Red
VC	Vibrational Coherence

# ABSTRACT

Raman spectroscopy has revolutionized molecular spectroscopy especially coming to the fields of biology, material science and analytical chemistry. Stimulated Raman techniques overcome the limitations that exist in spontaneous Raman spectroscopy where the time bandwidth relationship of Raman excitation pulse hinders tracking of structural events in ultrafast time scale. Impulsive Stimulated Raman Spectroscopy (ISRS) is one such technique that is used to track nuclear dynamics with femtosecond accuracy. The vibrational wavepacket evolving in both excited and ground state of small molecules is studied using ISRS to learn more about the vibronic photophysics of chemical systems. The technique helps to observe nuclear dynamics of Raman active vibrational modes from terahertz to larger wavenumbers with considerable sensitivity. It also suppresses background signals easily which has plagued ultrafast vibrational spectroscopy for decades and also resonantly enhances the signal-noise ratio of Raman spectra. In ISRS, time domain signal raw data is truncated and Fourier transformed to get information on the normal modes of vibration.

We use sub-femtosecond pulses to spectrally disperse the ISRS data in the visible region due to complexity in generation and management of temporarily short pulse in UV/IR region. methylene blue, Nile blue and 4-dimethylamino-4'-nitrostilbene (DNS) molecule were selected as potential candidates keeping in mind the presence of low frequency modes which becomes difficult to observe using already well established frequency resolved FSRS due to Rayleigh scattering .

DNS complex is utilized to study Twisted Intermolecular charge transfer (TICT). TICT is defined as a dual fluorescence phenomenon in which torsional change takes place in excited state from a planar locally excited conformer to a perpendicular CT conformer, following electronic excitation. The coupled vibrational modes of TICT molecules are analyzed to describe twist in excited electronic state. We employ computational calculations using DFT and TD-DFT level of theory to observe nature of potential energy surface and to calculate the vibrational spectra in both ground and excited state on other known TICT molecules. Using both impulsive stimulated spectroscopy and ab-initio calculations we try to create a clearer picture on how chemical system evolves.

# CONTENTS

List of figures

List of tables

Abbreviations

Abstract

Chapter 1: Twisted Intramolecular Charge Transfer (TICT)	16-22
1.1 Introduction	17-18
1.2 Properties of TICT	18-22
1.2.1 Solvent Polarity	19-20
1.2.2 Orientation along molecular backbone	21-22
1.3 Application of TICT	22
Motivation	23
Chapter 2: Spectroscopic techniques for the study of chemical systems	24-34
2.1 Introduction	25
2.2 Ultrafast Spectroscopy	25-33
2.2.1 Transient Absorption Spectroscopy signals (TAS)	27-28
2.2.2 Impulsive Stimulated Raman Spectroscopy (ISRS)	28-31
2.2.3 Time-Resolved Impulsive Stimulated Raman Spectroscopy (TR-ISRS)	32-33
2.3 Computational Chemistry	33-34
2.3.1 Density Functional Theory (DFT)	34
2.3.2 Time Dependent Density Functional Theory (TD-DFT)	34
Chapter 3: Tracking structural dynamics of polyatomic molecules using ISRS and TD-DFT	35-47
3.1 Introduction	36
3.2 ISRS of polyatomic molecule	36-41
3.2.1 Experimental method	36-37

3.2.2 Results and Discussion	37-41
3.3 DFT and TD-DFT calculation on polyatomic molecule	41-48
3.3.1 Computational method	41-42
3.3.2 Results and Discussion	43-48
Chapter 4: Excited state and ground state structural dynamics of TICT molecules	49-62
4.1 Introduction	49
4.2 TICT in DMABN molecule	50-55
4.3 TICT in DMPNA molecule	56-57
4.3 TICT in DNS molecule	57-62
Conclusion	63
Bibliography	64-66

# **Chapter 1**

## Twisted Intramolecular Charge Transfer (TICT)



## 1.1 Introduction

Twisted Intramolecular charge transfer (TICT) is a charge transfer process that occurs during photoexcitation in molecules that contain a D-A (donor-acceptor) pair covalently linked either by a single bond or  $\pi$  bonded backbone (D-B-A) system. This covalently linked donor-acceptor conjugated molecules undergo intramolecular charge transfer mediated by a structural relaxation in the excited state adiabatic photo surface via a twist in the molecular backbone. This twist alters the pi-conjugation that exists in the excited state and hence brings about change in photophysical properties of corresponding fluorescent molecules <sup>[1]</sup>.

This twist around a single bond produces a relaxed perpendicular structure from a previously stable locally excited (LE) conformation. The equilibrium between these two conformations results in a unimolecular dual fluorescence phenomenon. In order to understand the formation of the twist, a molecular orbital approach is required. Following a vertical excitation from the Franck Condon geometry of fluorophore in ground state ( $S_0$ ), a locally excited state is attained. This electronic charge transfer state ( $S_1$ ) involved in the fluorophore also contains an ET (electron transfer) character along with the LE (locally excited) character (see Figure 1.1). The adiabatic electronic potential states along the twisting reaction coordinate are formed as a linear combination of this ET and LE states [2]. The D-A systems that shows TICT contains frontier orbitals where electron transfer take place from the donor orbital (HOMO) to acceptor orbital (LUMO) resulting in a biradicaloid pair. Frontier orbital interaction increases the excitation energy and in order to minimize this excess energy, the system relaxes to a twisted conformation which corresponds to a dominant ET character.

The existing notion of describing the LE state is having a planar geometry with respect to the molecular axis. Going by this description, the equilibrium that exists between the planar and perpendicular (twisted) D-A conformation dictates the coefficient of ET and LE character of the  $S_1$  state. The dual fluorescence property corresponds to the formation of a second minimum in the  $S_1$  state, where the ET state overweighs the LE state upon twist in molecular backbone. Following the formation of this new local minimum, the  $S_1$  charge transfer state is represented as a TICT state. Understanding the factors that influence the equilibrium and hence the coefficient of LE and ET state that make up the  $S_1$  electronic state will give a better control in exploring TICT and helps to exploit it in different applications in chemistry.

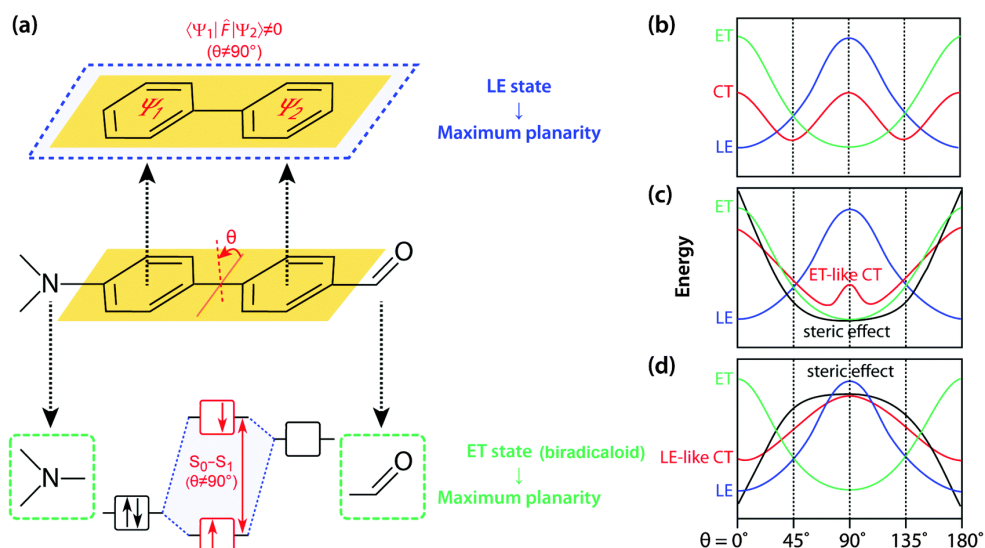


**Figure 1.1:** a) Schematic diagrams of the  $^1LE$  (blue),  $^1ET$  (green) and  $^1CT$  (red) states when: (b)  $^1LE$  and  $^1ET$  character are comparable to each other, (c) when the steric restriction (black) is introduced to twist the D–A junction (e.g. an alkyl group at ortho-position) and (d) when the D–A junction is made coplanar<sup>[2]</sup>.

## 1.2 Properties of TICT

The double fluorescence is what attracted attention of various research groups into looking at various D-B-A/D-A system including Dimethylaminobenzonitrile (DMABN) which is one of simplest TICT systems. When a lot of researchers misunderstood the anomalous emission band to be due to an excimer formation in DMABN molecule (nitro group is donor, cyano group is the acceptor and benzene acts as the backbone), it was Dr. Grabowski & co-workers who predicted that a twisting in excited state is what results in the unusual red shifted second fluorescence band. When absorption happens, the fluorophore undergoes emission from the planar conformation with partial charge transfer characteristics. Following this structural relaxation, a twist in the D–A single bond also happens that leads to a perpendicular conformation. The red shifted emission band is formed corresponding to the TICT state. Grabowski & co-workers showed that a strong absorption band and lack of concentration dependence on intensity ratio of the two emission band meant that an excimer cannot be the

plausible reason for the fluorescence anomaly <sup>[3]</sup>. Various polarity and viscosity experiments were performed in order to show that a bond twisting charge transfer state is responsible for shifted fluorescence band.

### 1.2.1 Solvent Polarity

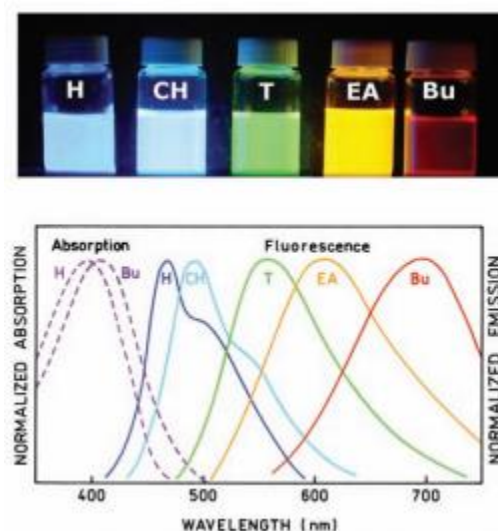


**Figure 1.2:** Photograph and emission spectra of DNS in solvents of increasing polarity. H, hexane; CH, cyclohexane; T, toluene; EA, ethyl acetate; Bu, n-butanol <sup>[4]</sup>.

The solvent polarity dependence and the associated shift in wavelength known as solvatochromism can be related to the solvent reorganization that follows twist in TICT molecules (see Figure 1.2). When solvent reorganization takes place in 10-100 picoseconds, it does not influence molecular absorption (with a timescale of  $10^{-15}$  sec) however it affects fluorescence which is a much slower process ( $10^{-9}$  sec). TICT active fluorophores have high excited state dipole moment and a much intense emission band corresponding to the TICT state in more polar solvents. Both of these properties can be better understood using Lippert-Mataga solvatochromic model.

$$\nu_F - \nu_A = \frac{2}{hc} \frac{\left( \frac{\epsilon - 1}{2\epsilon + 1} - \frac{n^2 - 1}{2n^2 + 1} \right) (\mu_E - \mu_G)^2}{a^3} \dots \dots \dots (Eq 1)$$

$$\left( \frac{\epsilon - 1}{2\epsilon + 1} - \frac{n^2 - 1}{2n^2 + 1} \right) = \Delta F \text{ (Orientation Polarizability)} \dots \dots \dots (Eq 2)$$

$$\nu_F - \nu_A = \frac{2}{hc} \frac{(\mu_E - \mu_G)^2}{a^3} \Delta F \dots \dots \dots (Eq\ 3)$$

Here  $\nu_F - \nu_A$  corresponds to the shift in frequency between absorption and fluorescence maximum,  $\mu_E$  is excited state dipole moment,  $\mu_G$  is ground state dipole moment,  $a$  is Onsager radius,  $\epsilon$  is dielectric constant of solvent,  $n$  is refractive index of solvent. The  $\frac{n^2-1}{2n^2+1}$  term corresponds to redistribution of electrons in the solvents, while the  $\frac{\epsilon-1}{2\epsilon+1}$  term corresponds to two factors, reorganization of solvent dipoles and redistribution of electrons in solvent. This effectively leaves us with orientation polarizability depending on reorganization of solvent dipoles as the later component effectively cancels off.

When  $\mu_E < \mu_G$  in the Eq 3, the ground state is stabilized by polar solvent and hence results in a hypsochromic shift, while in case of  $\mu_E > \mu_G$ , the excited state is stabilized by the polar solvent and a bathochromic shift is observed. In case of TICT molecules, the red shifted fluorescence band corresponds to presence of high dipole moment in excited state in highly polar solvents (see Figure 1.3).

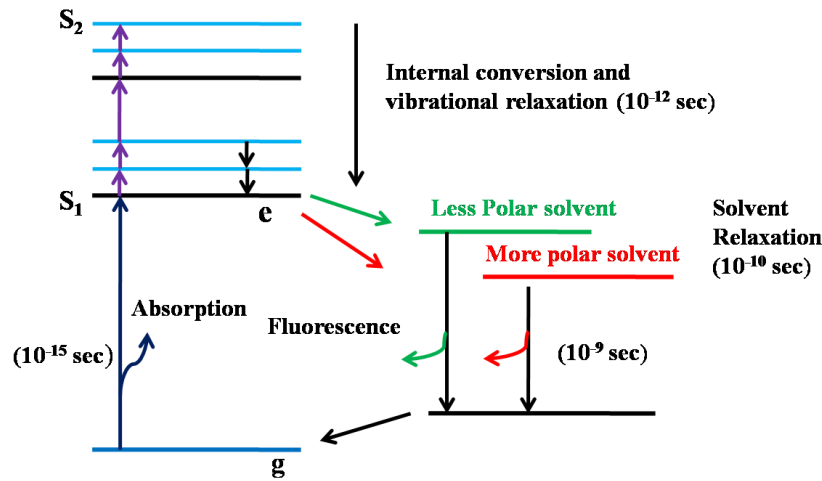


**Figure 1.3:** Jablonski diagram for fluorescence with solvent relaxation

### 1.2.2 Orientation along molecular backbone

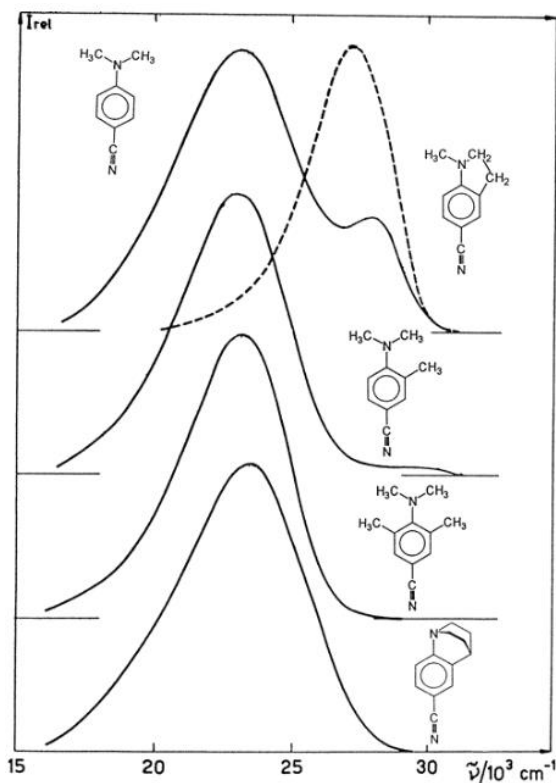


**Figure 1.4:** Fluorescence spectra of **DMABN** and the model compounds in  $\text{CH}_2\text{Cl}_2$  at  $25^\circ\text{C}$  <sup>[5]</sup>

The relative orientation of substitutions on the molecule influences the formation of the TICT fluorescent band. When the molecule is able to rotate freely around a single bond in the molecular framework from a planar conformation to the twisted one, the dual fluorescence band will have more intense characteristics. In case of DMABN for example (see Figure 1.4), the fluorescence spectra obtained in a polar solvent shows two emission bands with a more intense band corresponding to planar conformation and a less intense red shifted band corresponding to twisted conformation. The electronic spectra of other model compounds which are essentially substitutions made on DMABN parent complex show bands whose position keeps on shifting. Looking at excitation characteristics of molecule from the top to bottom fashion, in the first molecule the substitutions in the amino group are out of plane of benzene, resulting in molecule already in a twisted conformation, while the substitutions in

the ortho position of benzene ring slightly restricts rotation from a planar geometry. When a chelation is formed as in case of the last molecule, the molecule is constrained to a planar conformation alone and no twist can take place along D-A bond. The viscosity of solvent used can also add to the nature of twist that will take place along the backbone of the fluorophore.

### 1.3 Applications of TICT

TICT molecules have a wide range of uses and applications

**a) Solar energy conversion:** The pair of charges that are generated at the donor and acceptor ends of a TICT fluorophore following the photoexcitation during solar irradiation, corresponding to twist in the molecular backbone is collected and stored by using electrodes. The long lifetime of photoexcited state enabled by charge separation plays a major role in solar energy conversions <sup>[6] [7]</sup>.

**b) Polarity sensors:** Since TICT molecule behaves differently in polar and non polar solvents, by using them one can determine the relative polarity of an unknown solvent. The polarity of solvent dictates the stabilization of the TICT state through solvent reorganization. Hence they are ideal to be used as polarity sensors.

**c) Viscosity sensors:** The twist along the single bond in the molecular framework is also dependent on the viscosity of solvent medium and this makes them a candidate for viscosity sensors <sup>[8]</sup>.

**d) Chemo-sensors:** Utility of TICT molecule as chemo-sensors can be understood as being analogous to On-Off switch in the form of fluorescence of red shifted emission band following twist with change in the chemical environment and photoexcitation conditions <sup>[9] [10]</sup>.

## Motivation

In D-B-A molecular systems, theoretical investigation and quantum chemical calculation predicts both the localization and extent of twist induced structural change after charge transfer in the excited state. However a definite structural evidence for presence of TICT states in D-B-A system is missing, especially the twist in molecular backbone was never experimentally demonstrated with respect to the relevant electronic states.

Ultrafast Spectroscopy that temporally probes the atomic displacement with high bond specificity is suited to find the reaction coordinate(s) involved in driving the twist. Time resolved absorption and emission spectroscopy is used to study excited state evolution of D-A complex. However due to broad line width and convolution of congested electronic states, limited structural information is conveyed. Transient Vibrational Spectroscopy provides bond specific information on vibrational frequency and intensity following structural evolution in excited electronic state.

Time Resolved Impulsive Stimulated Raman Spectroscopy (TR-ISRS) and Impulsive Stimulated Raman Spectroscopy (ISRS) can be used to track reaction coordinate (s) that drive the formation of an Intramolecular Charge Transfer (ICT) manifold in multiple D-B-A molecular system.

# **Chapter 2**

Spectroscopic techniques for the study of  
chemical systems



## 2.1 Introduction

Ultrafast spectroscopy and computational chemistry works hand-in-hand to help understand static and dynamic effects in molecular chemistry. The present understanding of photochemistry on TICT molecules is limited in the exact nature of twist that takes place in the molecular framework that follows the charge transfer in the excited state upon photoexcitation. Linear spectroscopic techniques such as absorption and fluorescence spectroscopy can only give superficial picture about the dual fluorescence characteristics of the TICT molecule and its solvent polarity dependence.

Researchers to the present day hold varying arguments on the D-B-A charge transfer state. A 2D-potential well can be the best way out of all this to visualise the TICT phenomenon. A relative coordinate involving a change in bond length combined with a twisting dihedral is often seen as manifestation of the formation of charge transfer state. We are essentially trying to capture this image using ultrafast spectroscopic techniques.

The evolution of molecule along the slope of this well can be captured by Impulsive Stimulated Raman spectroscopic experiments. The investigation is systemically supported using theory done using computational packages (Gaussian 09 software). Density Functional Theory (DFT) and Time Dependent Density Functional Theory (TD-DFT) is used in order to calculate ground and excited state internal properties of small molecules respectively.

A comprehensive study by drawing necessary inferences through correlation of theory and experiment is performed. Extensive literature has also been cross verified in order to come up with the methodology followed, which can be understood in a broad way by reading the sections of this chapter.

## 2.2 Ultrafast Spectroscopy

In our work Impulsive Stimulated Raman Spectroscopy (ISRS) and pump-probe/transient signals act as main tools to study the excited state structural dynamics of selected chemical systems. Transient absorption spectroscopy has become a powerful and widely used technique for the study of photochemical processes. In this method the process which is to be

investigated is triggered by exciting the molecule using ultra-short pulses with a controllable delay. In order to completely understand the structural changes that are involved in the formation of twist in TICT process, time domain Raman spectroscopic techniques like ISRS needs to be employed, found correlated with pump-probe transients.

Knowledge of the electronic signature in TAS is essentially needed before venturing into Impulsive Stimulated Raman Spectroscopy (ISRS). Transient Absorption Spectroscopy involves exciting the sample with a short laser pulse (called pump) and monitoring the changes by another time delayed pulse (called probe). The dynamics of electronically excited states is probed to monitor the photo-induced transmission changes in the system. The delay between the pump and the probe is varied using a mechanical delay line. Every alternate pump pulse is blocked using a chopper running at half the frequency of the laser. The absorbance of the probe is then taken both in presence and in the absence of pump. The difference of these two absorbance data gives the required transient absorption signal (see Figure 2.1).

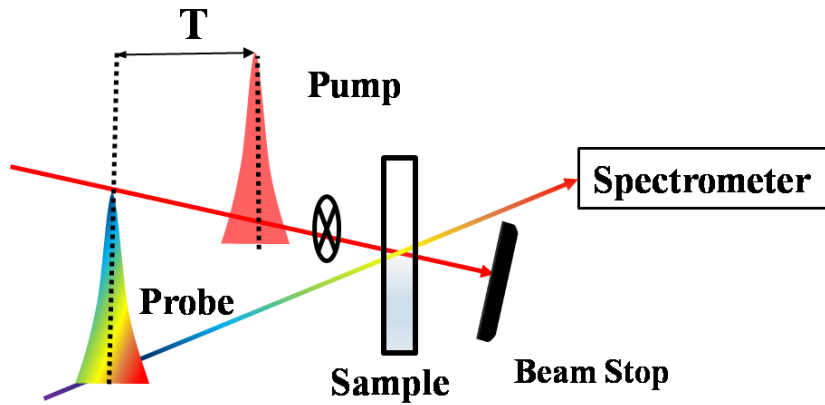


*Figure 2.1: Schematic of a pump – probe experiment*

The differential absorption signal is given as:

$$dOD(\lambda, T) = \left( -\log_{10} \left( \frac{OD \text{ probe/ pump on}(T, \lambda)}{OD \text{ probe/ pump off}(\lambda)} \right) \right)$$

### 2.2.1 Transient Absorption Spectroscopy signals

The transient absorption signal of a molecule can contain three types of signals which are:

- (1) Ground State Bleach (GSB)
- (2) Stimulated Emission (SE)
- (3) Excited State Absorption (ESA)

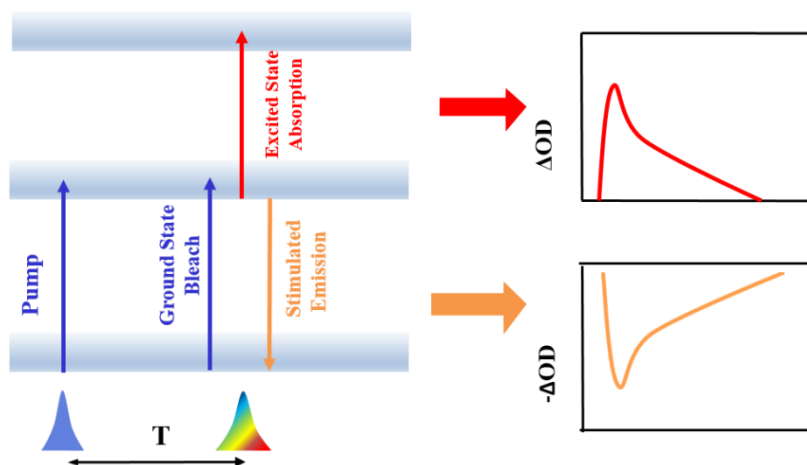


*Figure 2.2: Types of signals in a pump – probe experiment*

- 1. Ground State Bleach (GSB):** On exciting the sample with the pump, the ground state population is depleted. Therefore, the absorption of the probe at wavelength of ground state absorption is decreased and thus a negative differential absorption ( $\Delta OD$ ) is seen. This signal is called as ground state bleach (GSB).
- 2. Stimulated Emission (SE):** The probe can stimulate the population in excited state (created by pump) back to ground state. When the pump is blocked, the number of photons reaching the detector is the total photons contained in the probe. When the pump is on, the number of photons reaching the detector is the number of photons in the probe plus the photons emitted by the sample. Thus,  $I_{pump\ on} > I_{pump\ off}$ . Therefore a negative differential absorption ( $\Delta OD$ ) signal is observed. This signal is called as stimulated emission (SE).

3. **Excited State Absorption (ESA):** The molecule in its excited state can absorb a photon from the probe and go to a higher lying excited state. In this case  $A_{\text{pump on}} > A_{\text{pump off}}$  and a positive differential absorption ( $\Delta OD$ ) signal is seen. This signal is called as excited state absorption (ESA).

## 2.2.2 Impulsive Stimulated Raman Spectroscopy

Both the Infrared and Raman approaches in vibrational spectroscopy have contributed in understanding structural dynamics of molecules. Resonance enhancement of vibrational signatures is a characteristic property of Raman Spectroscopy which can be exploited to different experiments setup in linear and non-linear regimes. There are different non-linear spectroscopic techniques like Coherent Antistokes Raman Spectroscopy (CARS) and Femtosecond Stimulated Raman Spectroscopy (FSRS) which are suitable in understanding structural dynamics [11]. However for experiment requiring better time resolution, Time resolved Impulsive Stimulated Raman Spectroscopy (TR-ISRS) and Impulsive Stimulated Raman Spectroscopy (ISRS) are seen to be better than former.

In ISRS, the data is obtained in the time domain and is then Fourier transformed into frequency domain to obtain necessary normal modes of motion.

### 2.2.2.1 Theoretical Understanding

Impulsive Stimulated Raman Spectroscopy (ISRS) traces its origins to the very idea that led to discovery of Raman effect. Scattering of light following quantised vibrational states, when a photon excites a molecule from ground vibrational state ( $v = 0$ ) to a higher imaginary state and finally de-excites to a higher vibrational state ( $v = 1$ ) of the same electronic state, leaving a photon behind to be analysed is ISRS described in Layman terms.

In broader terms, ISRS is a third order non linear process  $\chi^{(3)}$ , where an ultrashort pulse (pump) interacts twice with the molecule. Initially the field interaction  $E_1$  takes the system into a high lying virtual state and as the pump interacts again with the molecule; the field interaction  $E_2$  de-excites the system to a higher energy vibrational state. This results in formation of vibrational coherence (VC) as a superposition of various vibrational levels that evolves along the ground potential energy surface (PES) (see Figure 2.2). The coherence

oscillates at time scale corresponding to the characteristic Raman active mode and has a dephasing time of few picoseconds. These vibrational oscillations can be recorded in a pump-probe fashion and the vibrational modes of motion can be used to understand the structural dynamics involved by combining with other computational calculations. It is also important that the pump-probe bandwidth used for the experiment be sufficiently low in order to effectively superimpose multiple vibrational eigenstates at the same time ensuring high temporal resolution through time domain recording of data.

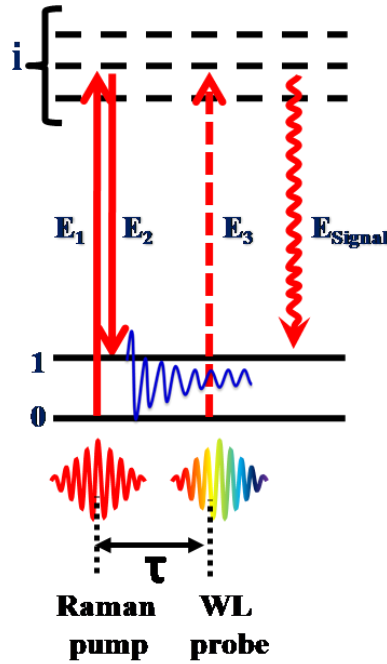


**Figure 2.3:** Energy level diagram showing the pulse sequence in ISRS involving electric field interactions from Raman pump and probe.

The vibrational wavepacket generated is probed using a field interaction  $E_3$ , generating a signal pulse ( $E_{\text{signal}}$ ) in optical phase-matching condition in self heterodyned manner to the broadband white light probe. The signal is then collected in a spectrally dispersed fashion, analyzed using functions in MATLAB (described in later chapters) and finally Fourier transformed from time to frequency domain [12].

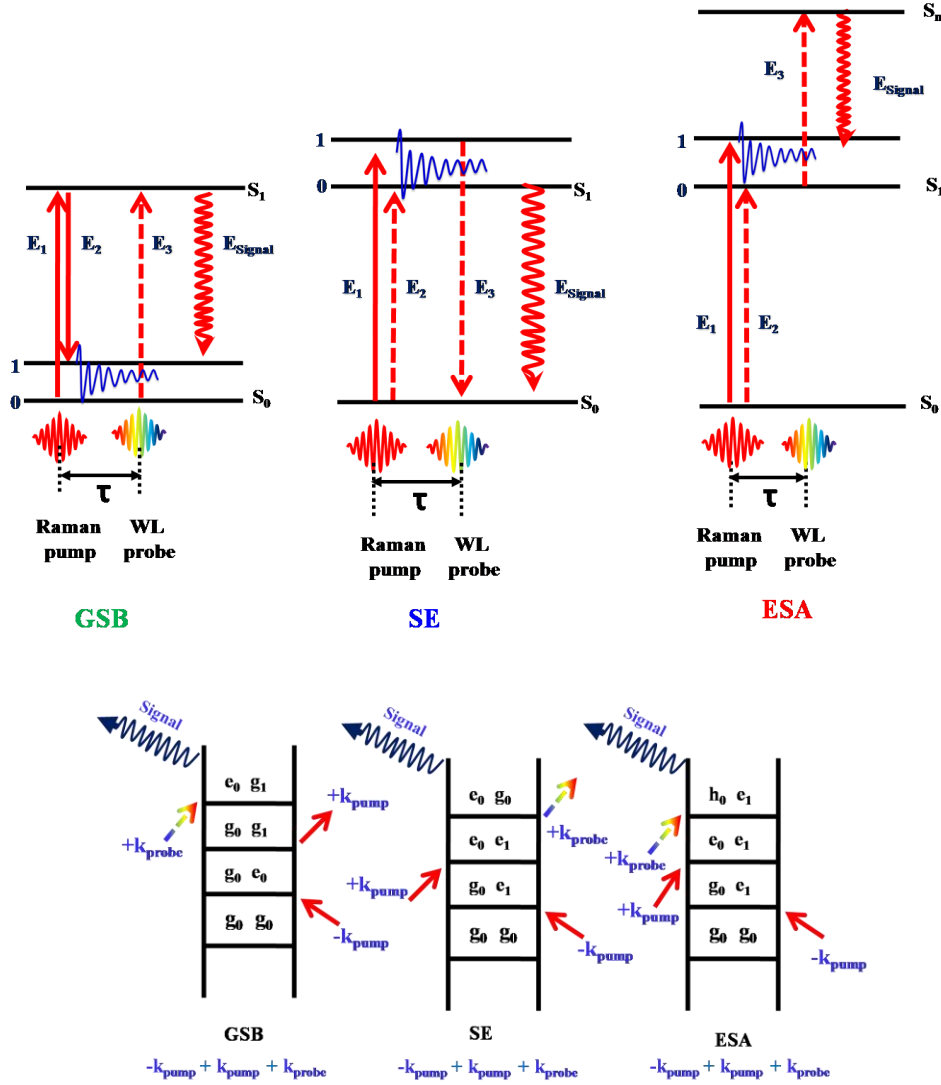


**Figure 2.4:** Energy level diagrams showing the pulse sequence in resonant ISRS corresponding to each electronic transient (top) followed by double sided Feynman diagram that shows the phase matching condition for each of the third order Liouville pathways.

When the virtual state lies closer to optically bright states, a resonant Raman signal is obtained overlapped with pump-probe transients. In this resonant ISRS condition, the VC evolves in the excited state (see Figure 2.3) unlike the ground state wavepacket generated in the nonresonant condition mentioned previously. However in resonant condition, the vibrational modes of excited state cannot be distinguished from the ground state modes even

after separating the electronic transient contribution. This is because the VC is also created in the ground state also along with the excited PES.

### **2.2.2.2 Specifications of the Instrument**

For our experiment Ti – Sapphire amplified laser beam was used to generate wavelength which was centred at 800 nm. The repetition rate and the pulse width of the laser were 1 kHz and 50fs respectively. In order to split the 800nm laser beam into pump and probe pulses a beam sampler was used in the path. Then probe pulse was routed to the custom-made femtosecond transient absorption spectrometer (TAS, Newport Inc, USA) which was further re-designed according to the specific requirement and pump pulse was routed toward the NOPA (Light Conversion) in order to get required wavelength for pump excitation. Pump and probe polarization both are vertical and parallel to each other, with a power of 1 mW and  $< 10 \mu\text{W}$  respectively. To generate the broad continuum of light in visible and near IR range sapphire crystal was used which was placed on a motorized translation stage. Intensity of probe pulse was controlled by variable neutral density filter at the sample position. 500 nm-700nm excitation wavelengths were generated using NOPA. To block every alternate pump pulse a mechanical chopper (New Focus 3502, with a 7/5 slot wheel, Newport Corp) was placed in pump arm which was operating at the 500 Hz repetition rate. Probe was spectrally overlapped with the pump beam, collimated and sent into the spectrograph (Oriel MS260i, Newport Corp). The transmitted probe pulse was detected with a spectrometer using 300 grooves/mm grating (Richardson grating 74064, Newport Corp) with the help of a linear array detector (CMOS S10453-1024Q, Hamamatsu Photonics). The time delay between the pump and probe pulses could be varied using a mechanical delay line (ILS300LM, Newport Corp) which was controlled by the software. The spectrally dispersed data is collected, analyzed and then Fourier transformed to obtain Raman modes.

### 2.2.3 Time resolved- Impulsive Stimulated Raman Spectroscopy

Since separating excited and ground state contribution of coherences is not easy using resonant ISRS experiment, unless the data collection is done in frequency dispersed manner and to maintain a pronounced control over the excited state structural dynamics, we employ TR-ISRS, where an additional pulse called actinic pulse is introduced before the Raman pump to take the system to a higher electronic state.

Through this process at different delays between the Raman and actinic pump, we obtain Raman snapshots of system evolving in the excited PES. The photophysics following this excitation to higher electronic state is similar to ISRS experiments.

Now coming to the experimental conditions needed for the experiment, an actinic pump is introduced in the pre existing ISRS setup. Mechanical chopper along the actinic arm and Raman pump arm has repetition rate of 500 Hz and 250 Hz respectively helping to create delay between pulses.

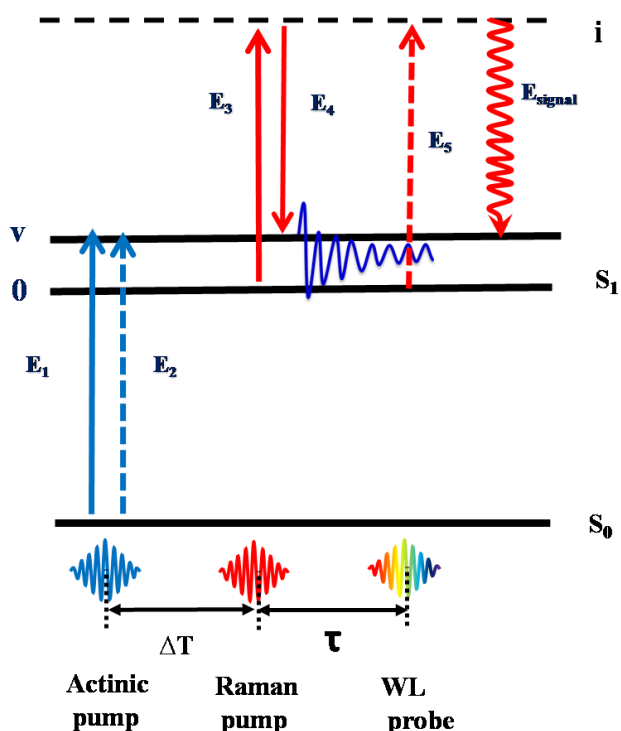


**Figure 2.5:** Energy level diagram for TR-ISRS experiment.



In TR-ISRS experiment, the actinic pump interacts twice with sample (field interactions  $E_1$  and  $E_2$ ) and this takes the system to the first excited state. Now with a delay ( $\Delta T$ ) w.r.t to the actinic pump, a second pulse known as Raman pump interacts with the electronically excited sample, creating coherence between the vibrational levels of the first excited state (see Figure 2.5). This coherence that evolves is then probed using a white light and scanned at delay  $\tau$  with respect to the Raman pump. The fifth order ( $\chi^{(5)}$ ) process is then studied in a spectrally dispersed fashion by analyzing the signal which is self heterodyned with the probe pulse with virtue of momentum conservation of fields known as phase matching.

In order to properly capture the  $S_1$  state coherence initiated by the Raman pump alone, an experimental procedure involving the record of four transient absorption maps is formulated. These wavelengths resolved maps plotted as a function of  $\tau$  is obtained by using two choppers running at different speeds to acquire data with and without actinic pump; with and without Raman pump, to subtract the background signals to get excited state Raman modes. The data analysis for TR-ISRS to obtain the vibrational modes of motion in excited state is similar to that of ISRS experiments. The snapshots of vibrations at every  $\Delta T$  will show the system evolves along the excited electronic PES and hence gives a better control over the structural dynamics of molecular systems following photoexcitation.

## 2.3 Computational Chemistry

By incorporating theoretical chemistry with computer simulations, solving complex chemical systems including their minima and transition state geometries along with other mechanical properties have become very easy. Broadly speaking about computational tools used in calculations, we tend to classify them as Molecular Mechanics (MM) and as Quantum Mechanics (QM). There are also problems which often require a hybrid QM/MM approach to effectively simulate the system.

Working in the regime of QM, we come across numerous ab-initio, semiempirical and density functional methods. For our work, we have used DFT in order to study the vibrational and electronic properties of molecules in the ground state. TD-DFT, a much more

advanced method in computational chemistry provided with a picture on the excited state of chemical system.

In order to support the experimental results obtained, computational calculations using Density Functional Theory (DFT) and Time Dependent-Density Functional Theory (TD-DFT) provides excellent grounds to understand the structural dynamics involved during TICT. These calculations were carried out by using Gaussian09 computational package. The initial geometry for ground state optimization was obtained by using Gaussview GUI software and optimising at a lower 3-21g\* basis set.

### **2.3.1 Density Functional Theory**

DFT theory holds its origin from Hohenberg- Kohn theorem (HK) which demonstrates ground state properties of many body systems with  $N$  electrons and  $3N$  spatial coordinates <sup>[13]</sup>. It reduces the problem into 3 spatial dimensions with the use of functional which encapsulate electron density. The many body system of electrons which are present in a static potential is replaced by a effective potential filled with non interacting particles that mimics the electrons. This potential contains both external and internal interactions, in the form of exchange and correlation interactions.

Dispersion effects are something that plagues DFT calculations over the years. This can be taken care by using necessary alternations to the exchange and correlation terms with different functionals.

### **2.3.2 Time Dependent Density Functional Theory**

Based upon Runge-Gross (RG) theorem <sup>[14]</sup>, TD-DFT can be seen as an analogue of the DFT in a time dependent external potential of a system. No minimization principle is used in TD-DFT unlike DFT. It can be used to describe excited states and is effective in extracting features like excitation energy, frequency dependent properties and absorption spectra.

# **Chapter 3**

Tracking structural dynamics of  
polyatomic molecules using ISRS and TD-  
DFT

## 3.1 Introduction

The research was done systematically by looking at the ground state properties using a combination of ISRS and DFT computations. Even though our basic question is regarding structural dynamics of TICT molecules; we acquire the language to describe this by looking at systems with simpler photophysics. Nile blue and methylene blue are some classic dyes that have interesting chemistry, ideal in terms of the photo absorption range and characteristic Raman active modes.

All spectroscopic experiments are performed by screening the suitable solvent system using relative solubility effects in which methanol seems to be ideal solvent for both the dyes. The molecules selected are also simple enough to encompass the computational cost of TD-DFT calculations.

## 3.2 ISRS of polyatomic molecule:

### 3.2.1 Experimental method

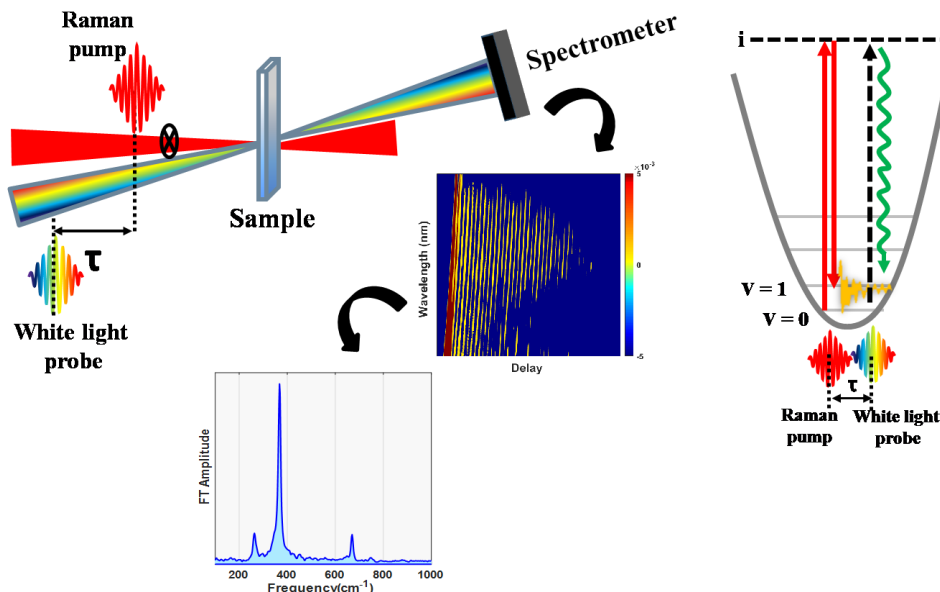


**Figure 3.1:** The experimental set-up for non-resonant ISRS along with a scheme for obtaining Raman spectrum

A schematic diagram for the ISRS experiment is shown above (see Figure 3.1). The experiment is performed using a femtosecond transient absorption spectrometer (Newport). A Raman pulse centred around 690 nm and 650 nm are generated with the help of a Non-collinear Optical Parametric Amplifier (Topas White, Light Conversion) pumped by Coherent Libra titanium-sapphire regenerative amplifier produced laser pulses centred on 802 nm, ~45 fs FWHM pulse width and repetition rate of 1KHz. The path of laser is split in order to generate the white light (WL) probe pulse by shining it on a sapphire crystal. Much more detailed information on the instrumentation can be understood by looking at section 2.1.2.2.

Nile blue 690 perchlorate purchased from Exciton and methylene blue purchased from Sigma Aldrich are used without any further purification. Stock solutions of these dyes are made using methanol as the solvent, the necessary solvent dilution is selected by keeping an optical density of ~1.0 at absorption maxima in a cuvette of 1mm path length.

Raman pump pulse is used to photo excite the sample and a white light used to probe the system at regular interval with respect to the Raman pump through a mechanical chopper. The probe-pump spatially overlaps inside the sample and following this the pump is blocked behind the sample holder. Meanwhile the probe pulse along with the photophysical transient time domain signal, formed heterodyned with the former gets collected in a spectrally dispersed fashion. After recording the required data, further analysis is done along a slice corresponding to wavelength required. This raw data is fitted using exponential functions and finally Fourier transformed using MATLAB programming (version 2018b, Math Works).

### **3.2.2 Results and Discussion**

Steady state absorption studies are done to understand how Raman pulse and white light probe overlap and the nature of coherence created within the molecular system. The spectral bandwidth is around ~33nm which can cover vibrations upto ~1000 wavenumbers, considering the broad spectral wing. The Raman pump had a pulse width of ~31fs found using intensity autocorrelation.

### 3.2.2.1 Nile Blue

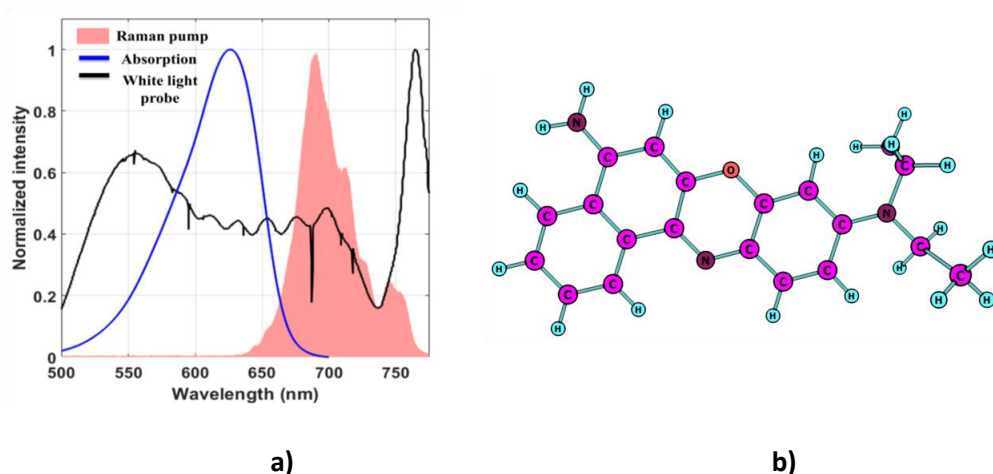


**Figure 3.2:** a) Absorption spectra of Nile blue (blue, solid line), Raman pump spectrum (red, filled plot) along with Gaussian fit (red, solid line) and WL probe spectrum (black, solid line) b) Molecular structure of Nile blue.

Nile blue has an absorption spectra spread around 625 nm and partially overlaps with the red edge with the Raman pump pulse used to photo excite the molecule. This resonance enhances the signal and at the same time makes sure that it remains dominated by ground state vibrational coherence. These vibrations are present correlated with a  $\Delta OD$  phototransients of pump-probe signal.

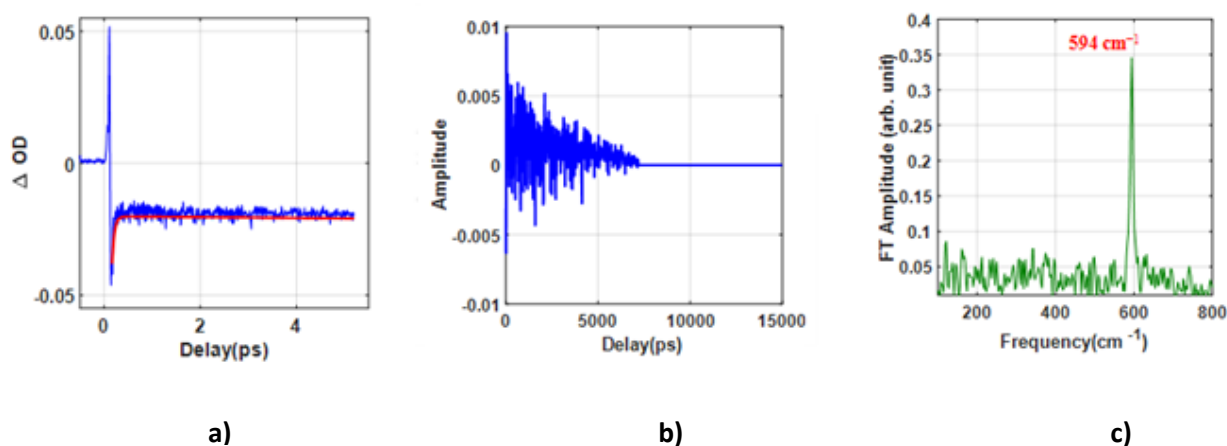


**Figure 3.3:** Time-domain data (blue curve) at  $\sim 625$  nm (GSB) recorded for Nile blue, polynomial fit to the data (red, solid line) (b) Processed data (blue curve) (c) Fourier transform of processed data giving Raman spectrum showing 594  $\text{cm}^{-1}$  mode.

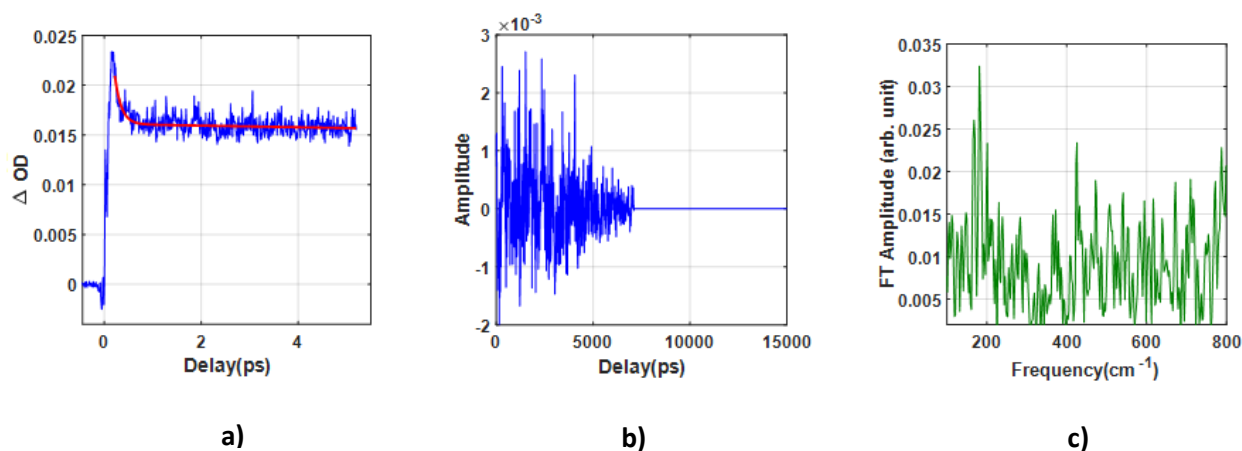


**Figure 3.4:** Time-domain data (blue curve) at ~530 nm (ESA) recorded for Nile Blue, polynomial fit to the data (red, solid line) (b) Processed data (blue curve) (c) Fourier transform of processed data giving Raman spectrum without any noticeable Raman peak.

The pump-probe transient of GSB (~625 nm) and ESA (~530 nm) is fit using a polynomial function and subtracted from the raw data to extract the coherent oscillations which corresponds to Raman active vibrations. Prior to this step, the coherent artifact<sup>[15]</sup> is skipped in signal analysis procedure. The residual is zero padded and windowed using Hanning function, finally Fourier transformed from time domain to frequency domain (see Figure 3.3 and Figure 3.4).

### 3.2.2.2 Methylene Blue

Methylene blue has a photophysics slightly different from Nile Blue, the absorption spectra of methylene blue (650 nm) overlap more significantly with the Raman pump centered on 650 nm (see Figure 3.5). The coherence hence evolves in both the ground and excited state and is studied using the resonant pump data and computational calculations.

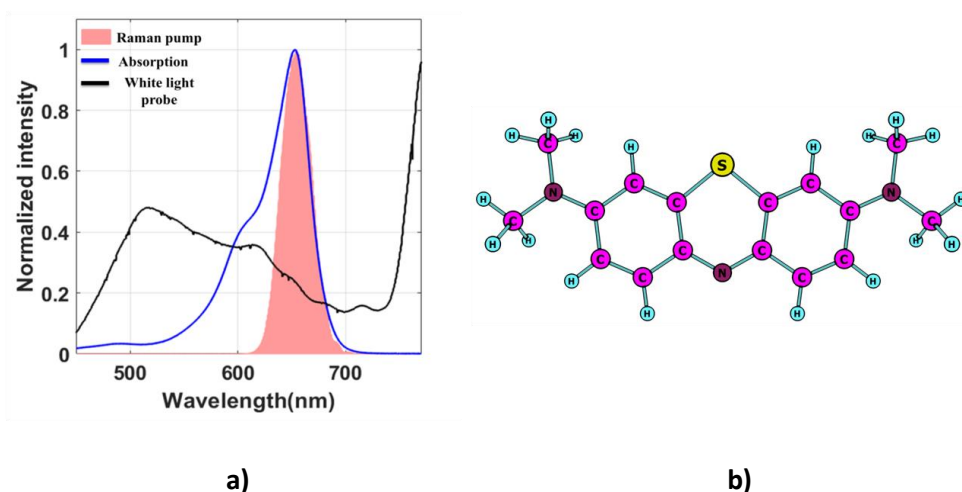


**Figure 3.5:** a) Absorption spectra of methylene blue (blue, solid line), Raman pump spectrum (red, filled plot) along with Gaussian fit (red, solid line) and WL probe spectrum (black, solid line) b) Molecular structure of methylene blue.

The Raman active vibrational modes below  $1000\text{ cm}^{-1}$  are obtained through similar scheme as one mentioned above for Nile blue. Methylene blue vibrational residue is extracted at both GSB ( $\sim 636\text{ nm}$ ) and ESA ( $\sim 581\text{ nm}$ ) unlike Nile blue coherence.

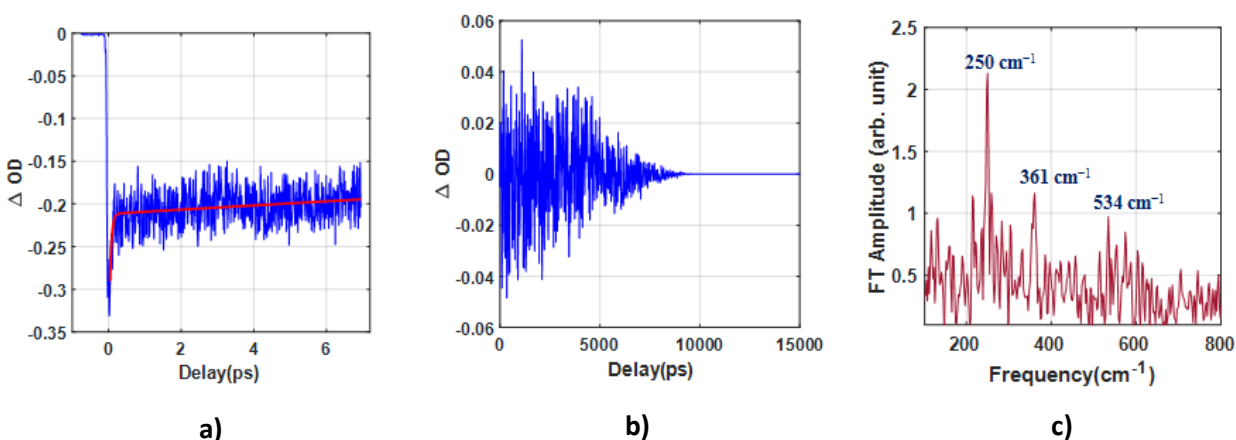


**Figure 3.6:** Time-domain data (blue curve) at  $\sim 636\text{ nm}$  (GSB) recorded for methylene blue, polynomial fit to the data (red, solid line) (b) Processed data (blue curve) c) Fourier transform of processed data giving Raman spectrum showing  $250\text{ cm}^{-1}$ ,  $361\text{ cm}^{-1}$  and  $534\text{ cm}^{-1}$  mode.



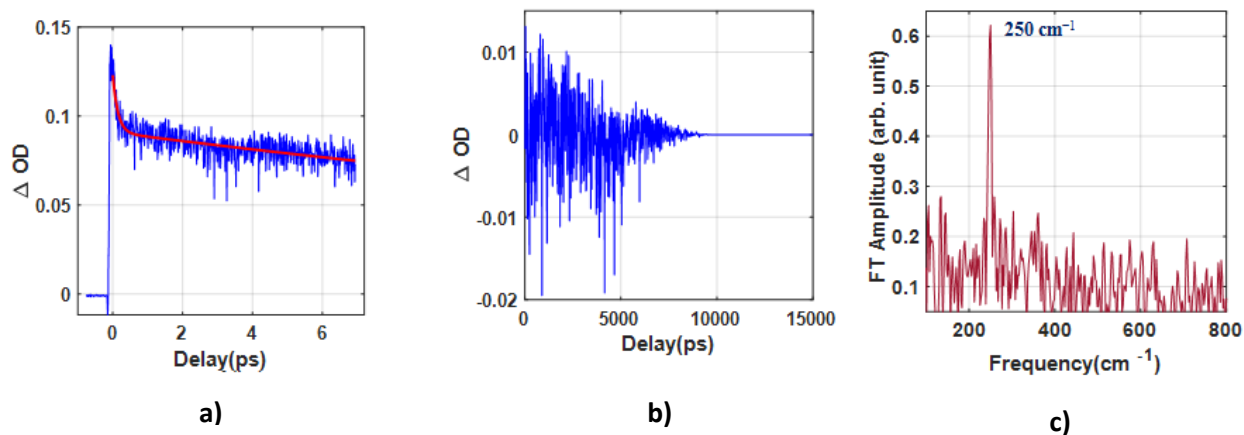


**Figure 3.7:** Time-domain data (blue curve) at ~581 nm(ESA) recorded for methylene blue, polynomial fit to the data (red, solid line) (b) Processed data (blue curve) (c) Fourier transform of processed data giving Raman spectrum showing 250 cm<sup>-1</sup> mode.

TR-ISRS experiment is done with a setup similar to ISRS (see section 3.1.A), an additional rail arm is introduced with a mechanical chopper to electronically excite the sample.

### 3.3 DFT and TD-DFT calculation on polyatomic molecules:

#### 3.3.1 Computational method

Nile blue and methylene blue ground state properties are studied using ground state geometry optimisation scheme and analytical frequency calculation at stable FC geometry available in Gaussian 09 package. The polarizability along the vibrational modes of motion is analysed to obtain the Raman activity spectrum. GaussSum python configured software is used in order to obtain the Raman intensity spectrum, which is used to compliment the experimental data.

$$I_i = \frac{f(\vartheta_o - \vartheta_i)^4 S_i}{\vartheta_i \left(1 - \exp\left(\frac{-hc\vartheta_i}{KT}\right)\right)} \dots\dots\dots (Eq 1)$$

Here the intensity  $I_i$  is represented in terms of linear scaling factor  $f$ , the frequency of pump used for exciting the sample ( $\nu_o$ ), the frequency of vibrational modes of motion ( $\nu_i$ ) and the temperature  $T$  in which experiment is performed. Here  $S_i$  is the Raman activity term which is calculated using Raman invariants of a vibrational polarizability tensor along a normal mode of frequency for a given molecule.

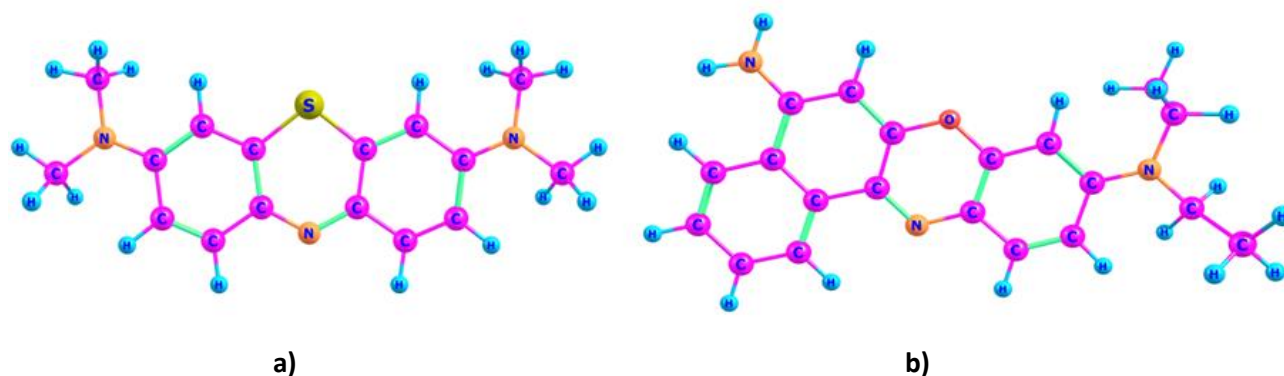


**Figure 3.9:** Ground state geometry of a) methylene blue and b) nile blue

Ground state calculations are performed for both gas phase and solution phase (methanol). The Raman and IR spectra for nile blue and methylene blue matches well with the experimental spectra obtained using ISRS. For nile blue, the basis set of choice is 6-31g+(d,p) which includes diffusive function necessary for atoms. The functional used is B3LYP as a 20% HF exchange is sufficient to reproduce the experimental data. Now for methylene blue, 6-311g++(d, p) is used as heavier sulphur atom is present and is identified in literature to be ideal basis for such molecules. Similarly, the choice of functional is also based on this heavier atom for which dispersion interaction is to be considered. M05-2X functional is used, as a portion of dispersion correction is taken care by the same and is ideal for later transition state search for TD-DFT calculations. Other functional considered includes M06-2X and wB97XD. The final choice is made by keeping expense of calculation, final geometry and simulated spectra in mind. The stabilized geometry is then screened for imaginary vibrational modes. For solvent phase calculation, IEFPCM solvent continuum model available in Gaussian09 is used.

## 3.3.2 Results and Discussion

### 3.3.2.1 Nile Blue

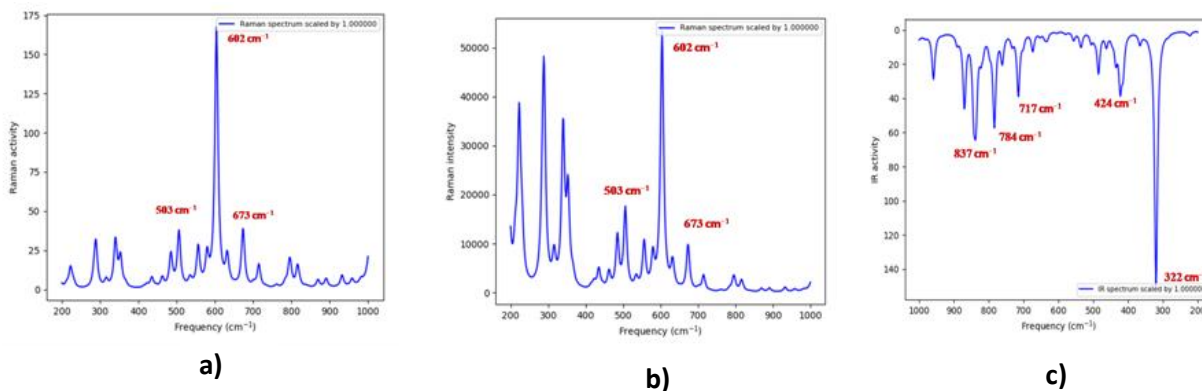


**Figure 3.10:** Simulated Ground state vibrational modes represented by a) Raman Activity spectra b) Raman Intensity spectra c) Infrared Intensity Spectra for Nile blue in gaseous phase obtained at 6-31+g(d,p) basis set and B3LYP functional (unscaled).

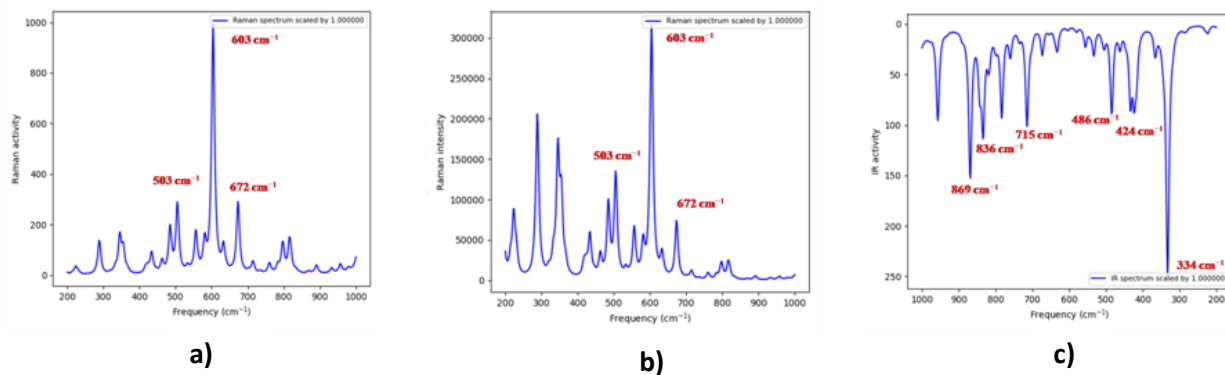


**Figure 3.11:** Simulated Ground state vibrational modes represented by a) Raman Activity spectra b) Raman Intensity spectra c) Infrared Intensity Spectra for Nile blue in solvent phase (methanol) obtained at 6-31g+(d,p) basis set and B3LYP functional (unscaled).

Characterization of the modes of motion is performed in Nile blue and simulated UV/Visible absorption spectrum is verified at the same point in the excited state potential surface. The

experimentally verified peak of maximum absorbance is 625 nm which is used as parameter for generating the Raman intensity spectra. (see eq 1)

No	Frequency (Gas Phase) (cm <sup>-1</sup> )	Frequency (Solvent Phase) (cm <sup>-1</sup> )	Frequency (Solvent Phase) (cm <sup>-1</sup> )(scaled 0.98)	Frequency (Experimental) (cm <sup>-1</sup> )	Characterization
1	602	603	592	594	Ring Breathing mode
2	673	672	659	--	Ring Wiggling mode

**Table 3.1:** Characterization of ground state vibrational frequencies of nile blue.

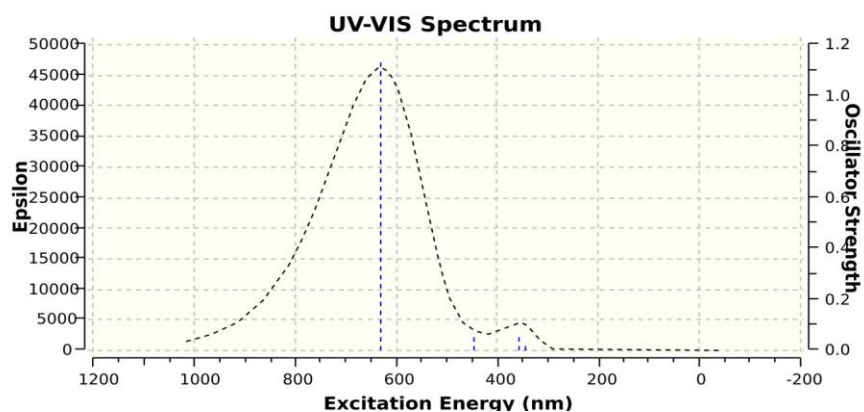


**Figure 3.12:** Simulated UV/Visible Absorption spectra for nile blue obtained at 6-311g++(d,p) basis set and M05-2X functional at solvent phase ( Maximum intensity at 625 nm) .

The UV spectra was generated by considering six low lying excited state ( more states not considered as it will be expensive in terms of computational time). Nile blue simulated

spectra overlap with our experimental spectra while a methylene blue maximum is slightly shifted with respect to the UV/Visible experiment.

In order to study the change of vibrational mode between ground and excited state of molecule, infrared spectra in ground and excited state is used. Since the vibrations in turn dictates the reaction coordinate along possible global minima, it tells us about structural dynamics in excited PES.

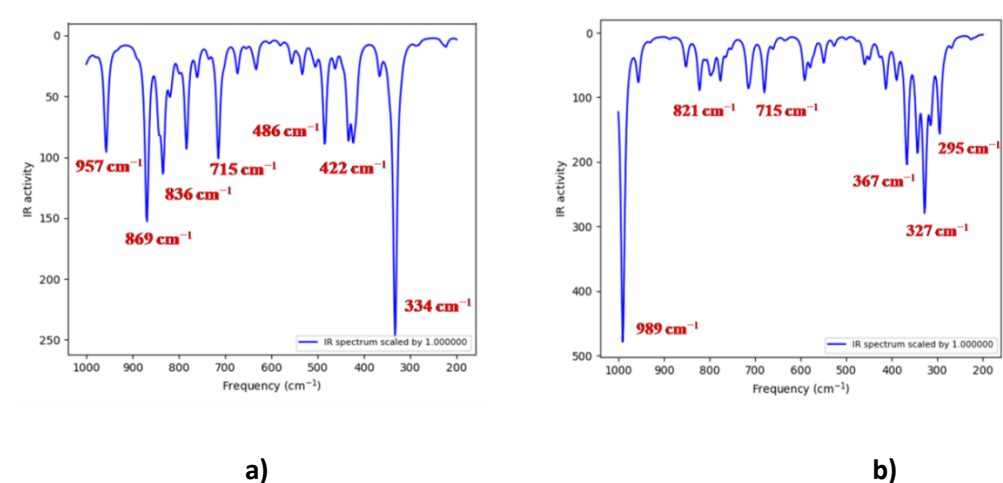


**Figure 3.13:** Simulated IR active vibrational modes of a) ground state spectra b) excited state spectra for Nile blue in solvent phase (methanol) obtained at 6-31g+(d,p) basis set and B3LYP functional

The vibrational frequencies in both ground and excited state seem to be having similar intensities and a slight shift in the value of frequency. Even though a qualitative analysis cannot be drawn from these calculations; quantitatively a blue shift of the modes can be realized.

Now in order to verify the experimental and theoretical Raman spectra obtained, we need to consider scaling the spectra by a factor with respect to the most intense experimental spectral frequency. In our case we have made sure the scaling required to analyse the experimental data is well in range of 0.98-1.02 factor.

The excited state frequency mode determination is computationally expensive as the frequency calculation in the excited state is done numerically compared to the analytical solution in ground state of the molecule. Raman activity value for excited state on the other hand is impossible to obtain using modules present in Gaussian 09.

### 3.3.2.2 Methylene Blue

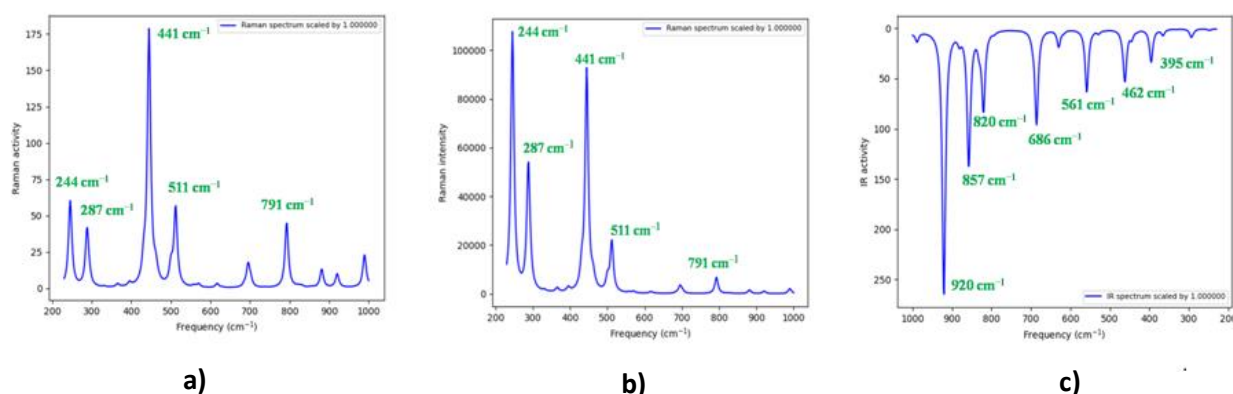


**Figure 3.14:** Simulated Ground state vibrational modes represented by a) Raman Activity spectra b) Raman Intensity spectra c) Infrared Intensity Spectra for methylene blue in gaseous phase obtained at 6-311g++(d,p) basis set and M05-2X functional (unscaled).

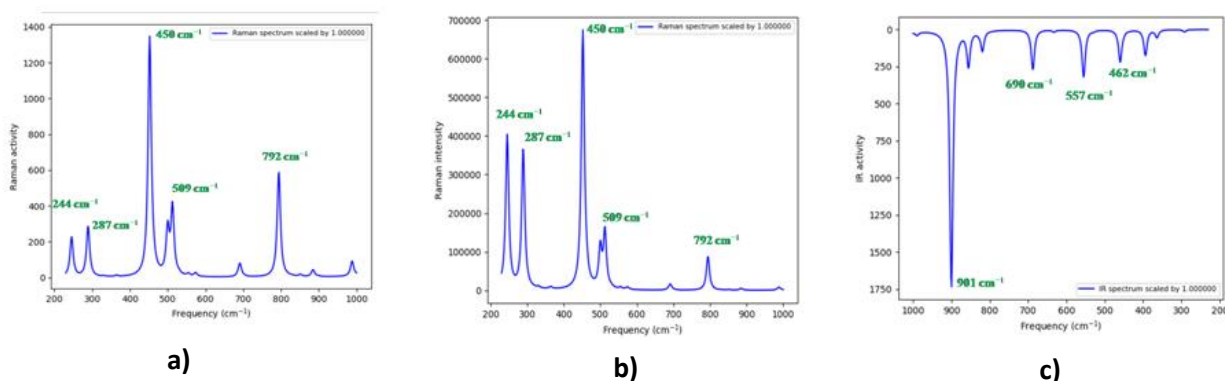


**Figure 3.15:** Simulated Ground state vibrational modes represented by a) Raman Activity spectra b) Raman Intensity spectra c) Infrared Intensity Spectra for methylene blue in solvent phase (methanol) obtained at 6-311g++(d,p) basis set and M05-2X functional (unscaled).

Methylene blue with an excitation wavelength of 650 nm has similar intensities for calculated frequencies in both gas phase as well as solvent phase (see Figure 3.13 and Figure 3.14). The simulated spectrum is then used to trace the frequency domain vibrational modes obtained during analysis of ISRS experimental data. The structural dynamics for the complex can be retrieved by observing the nature in which frequency shifts in excited state and corresponding characterization of these dominant Raman active vibrations.

No	Frequency (Gas Phase) (cm <sup>-1</sup> )	Frequency (Solvent Phase) (cm <sup>-1</sup> )	Frequency (Solvent Phase) (cm <sup>-1</sup> )(scaled 1.02)	Frequency (Experimental) (cm <sup>-1</sup> )	Characterization
1	244	244	249	250	C–N(CH <sub>3</sub> ) <sub>2</sub> stretching
2	441	450	461	--	CSC/CNC bending
3	511	509	521	534	CSC/CNC bending
4	791	792	808	--	CNC bending/C=C stretching

**Table 3.2:** Characterization of ground state vibrational frequencies of methylene blue.

The characterization is done using Gaussview software from the Gaussian09 frequency output file. The ground state geometry in the lowest point of potential surface well is utilized for a FC excitation to higher excited state. This is realised through a TD-DFT SCF calculation. For obtaining the UV/Visible absorption spectra,  $\epsilon$  vs  $\lambda$  (excitation wavelength in nm), the peaks assume a Gaussian band shape.

The calculation of the electronic spectra is performed at the same level of theory and basis set as that for the Raman spectra in order to maintain a standard reference throughout the calculations.

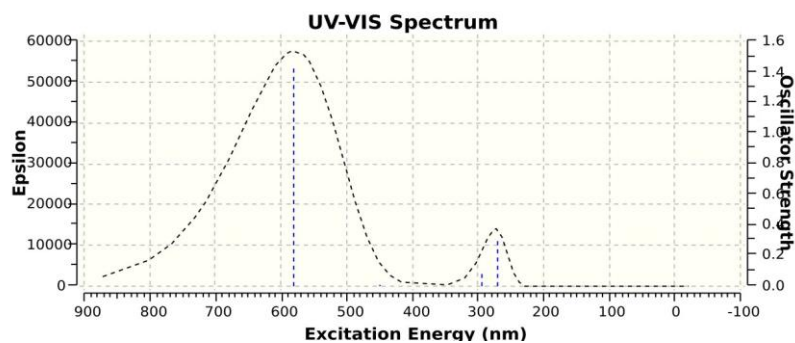


**Figure 3.16:** Simulated UV/Visible Absorption spectra for methylene blue obtained at 6-311g++(d,p) basis set and M05-2X functional at solvent phase ( Maximum intensity at 580 nm).

Similar to the case of nile blue, ground and excited state calculation were performed in case of methylene blue as well. The intensities of modes remain same while there is a shift in the frequencies of modes. This very well could be due to the rigid structure of nile blue and methylene blue.

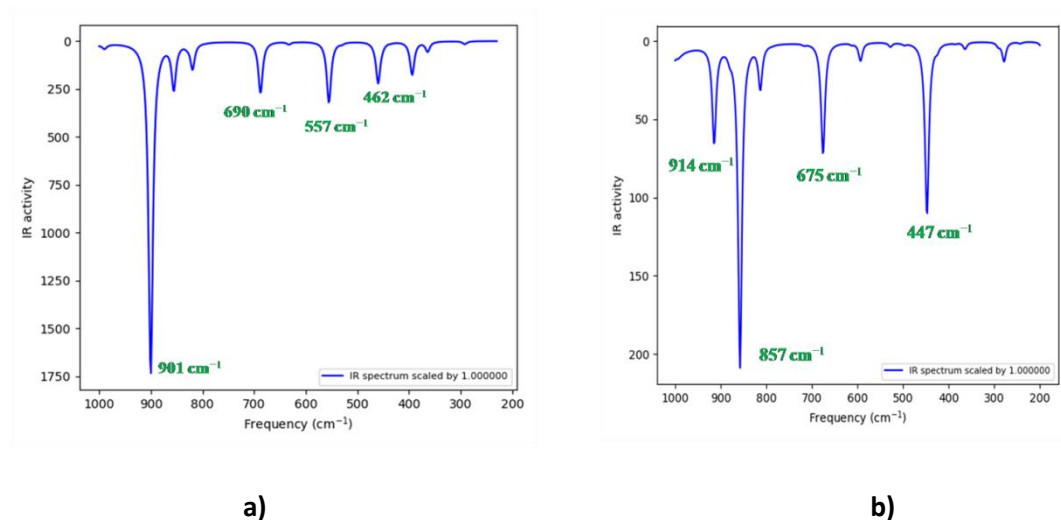


**Figure 3.17:** Simulated IR active vibrational modes of a) ground state spectra b) excited state spectra for methylene blue in solvent phase (methanol) obtained at 6-31g+(d,p) basis set and MO6-2X functional



# **Chapter 4**

Excited state and ground state structural  
dynamics of TICT molecules

## 4.1 Introduction

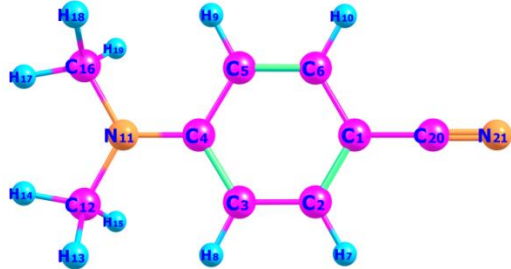
Similar to how ultrafast spectroscopy and DFT/TD-DFT is used to understand structural dynamics in dyes like nile blue and methylene blue, it can now be used to explore the twist along molecular backbone following charge transfer in the TICT molecules described in previous chapters.

We start of by looking at much smaller molecules like 4-(N,N-dimethylamino)benzonitrile (DMABN) and N,N-dimethyl-p-nitroaniline (DMPNA). Both are easier to work about computationally owing to the single bond rotation and rigid structure. From this picture gained, a much less explored problem on 4-dimethylamino-4'-nitrostilbene (DNS) is studied using both theory and experiment. DNS is an interesting case due to potential cis/trans isomerisation along with the twist along double bond of the stilbene complex.

## 4.2 TICT in DMABN molecule

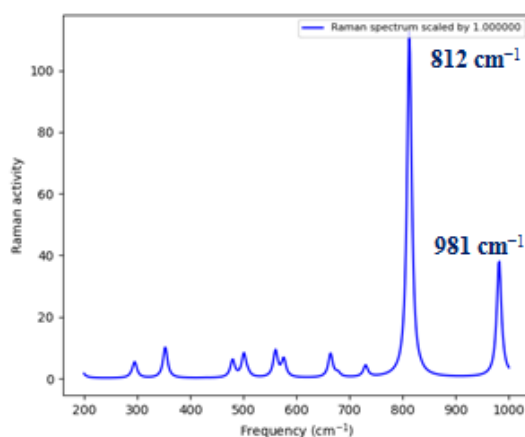
DMBAN molecule is the first TICT molecules to be studied in terms of a twist in the excited state that leads to the dual fluorescence characteristics. The molecule has a dimethyl amino donor moiety and a cyano group connected via a benzene ring spacer. The charge transfer characteristic is understood with the help of DFT/TD-DFT calculations.

The calculation is done with wB97XD functional, which is identified to be good while working with problems requiring inclusion of dispersion effects and charge transfer characteristics <sup>[16]</sup>. The ground state geometry is identified to be coplanar with respect to the plane of benzene ring (see Table 4.1).

<i>S<sub>0</sub></i> optimization			
			
<b>Dihedral C<sub>5</sub>-C<sub>4</sub>-N<sub>11</sub>-C<sub>16</sub></b>	3.541	<b>Bond length N<sub>11</sub>-C<sub>4</sub></b>	1.36378

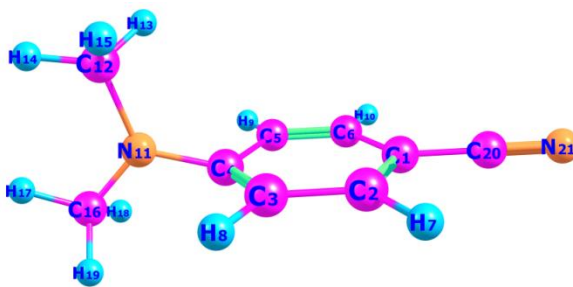
**Table 4.1:** Ground state geometry of DMABN optimized at wB97XD functional and 6-31g+(d,p) basis set using IEFPCM model of solvation containing a methanol dielectric.

Analytical frequency calculations and Raman intensity characterizations are made at the same geometry with the help of Gaussian09 and GaussSum software. The Raman and IR spectrum which is hence simulated in the ground state is used to track vibrational modes and how dynamics turn out in DMABN on photoexcitation.



**Figure 4.1:** Simulated Ground state vibrational modes represented by Raman Activity spectra for DMABN in solvent phase (methanol) obtained at 6-31g+(d,p) basis set and wB97XD functional (unscaled).

Now once the ground state frequencies are obtained with zero negative modes among them, using the same geometry, a vertical FC excitation is done using the TD-DFT scheme. The first excited state that is calculated is optimized and its frequencies generated using numerical method.

<i>S<sub>1</sub> optimization</i>			
			
<b>Dihedral C5-C4-N11-C16</b>	<b>-77.729</b>	<b>Bond length N11-C4</b>	<b>1.40141</b>

**Table 4.2:** Excited state geometry of DMABN optimized at wB97XD functional and 6-31g+(d,p) basis set using IEFPCM model of solvation containing a methanol dielectric.

In the excited state, the molecule is observed to undergo a twist in the molecular backbone. The –NMe<sub>2</sub> dihedral undergoes a planar to twisted conformation of around 80 degrees. (see figure 4.1 and figure 4.2). This twist is attained as the LE state overweighs the ET state following the HOMO-LUMO frontier orbital interaction that follows. This can be further understood by comparing the localization of molecular cloud among the donor –acceptors moiety upon exciting to the S<sub>1</sub> state. The electron cloud is seen to be delocalized in the S<sub>0</sub> state for both HOMO and LUMO while in the S<sub>1</sub> state, the LUMO\* has a charge localized in the donor dimethyl nitro end and HOMO\* in the acceptor cyano end. (see Figure 4.2)

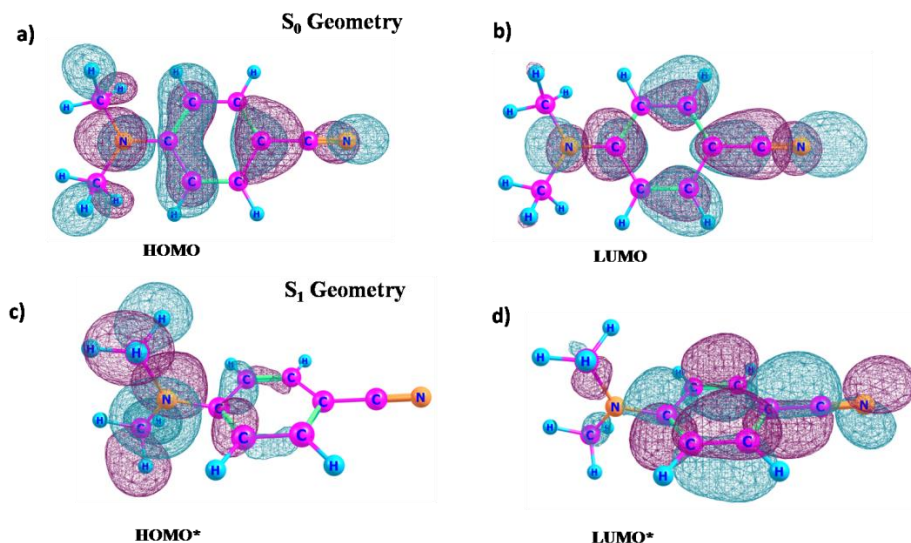


**Figure 4.2:** MO diagrams (isovalue 0.03) showing the flow of charge during vertical excitation and TICT formation a) HOMO b) LUMO of  $S_0$  planar geometry c) HOMO\* d) LUMO\* of  $S_1$  twisted geometry in DMABN, obtained at 6-31g+(d,p) basis set and wB97XD functional in methanol in IEFPCM model.

The molecular twist can be seen as a function of linear combination of vibrational modes of motion. Understanding what these bases are and contribution of each term of the basis as the molecule undergoes structural change from planar to twisted state is necessary. This can be done by looking at the IR/Raman activities of DMABN in the ground state and excited state.

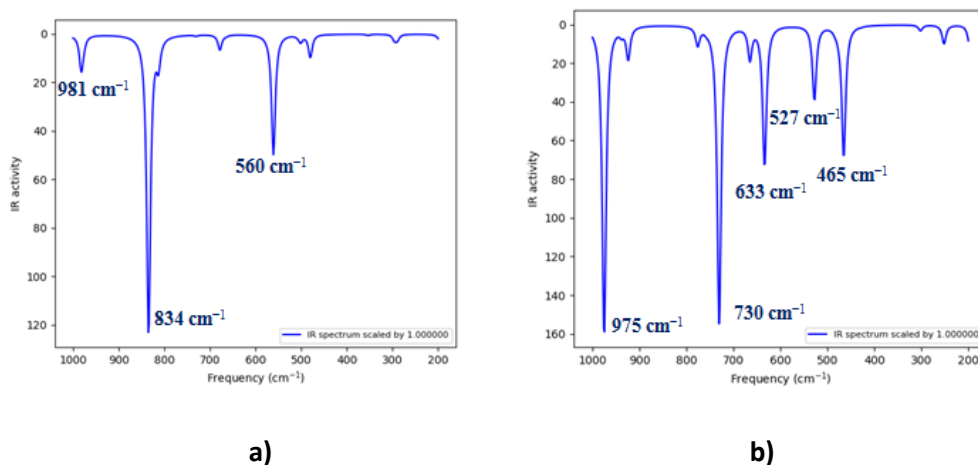


**Figure 4.3:** Simulated IR active vibrational modes of a) ground state spectra b) excited state spectra for DMABN in solvent phase (methanol) obtained at 6-31g+(d,p) basis set and wB97XD functional .

The vibrational modes are characterized in order to understand how the lower frequency modes shift and how other normal modes are involved in the formalization of the twist of the molecular backbone.

Ground state			Excited state		
No	Frequency (Solvent Phase) (cm <sup>-1</sup> )	Characterization	No	Frequency (Solvent Phase) (cm <sup>-1</sup> )	Characterization
1	981 cm <sup>-1</sup>	Ring breathing	1	975 cm <sup>-1</sup>	Ring breathing
2	834 cm <sup>-1</sup>	Ring H out-plane bend	2	730 cm <sup>-1</sup>	Ring H out-plane bend
3	560 cm <sup>-1</sup>	[Ring H out-plane bend + Cyano bend]+strong +[N(CH3) <sub>2</sub> rocking] weak	3	527 cm <sup>-1</sup>	[Ring H out-plane bend + Cyano bend]+strong +[N(CH3) <sub>2</sub> rocking] weak
			4	633 cm <sup>-1</sup>	Ring H in-plane bend + N(CH3) <sub>2</sub> rocking
			5	465 cm <sup>-1</sup>	Ring H out-plane bend + N(CH3) <sub>2</sub> rocking

**Table 4.3:** Ground and Excited state vibrational frequency characterization.

We observe a red shift in the vibrational modes in excited state, along with new modes that appear to be contributing to the excited state twist. The red shift in excited state can be ascribed to H-bonding or change in dielectric properties of environment. The ring breathing mode (981 cm<sup>-1</sup>) contribution decreases a lot while the rest of modes show no change in its intensity, which is expected as the bond rotation breaks the resonance along the benzene ring,

giving rise to uneven bond order symmetry axis along which the ring breathing mode is also manifested.

In case of DMABN, the vibrational coupled modes result in the dynamics along the  $S_0$  and  $S_1$  potential surface. The dihedral potential scan along the  $C3-C4-N11-C12$  axis gave us the electronic picture of TICT formation (see figure 4.3). A shallow minimum present in the  $S_1$  potential surface is observed and this barrier for TICT formation is identified to be  $\sim 0.24$  eV (from the FC geometry). This is very close to experimentally determined barrier of 0.28 eV in polar solvent <sup>[17]</sup>. TD-DFT relaxed scan confirms the small barrier in TICT formation. Similar calculations on higher excited states demonstrate a  $S_2/S_1$  conical intersection through which it relaxes to a TICT state <sup>[18]</sup>. However the CI seam is often incorrectly predicted in TD-DFT and discontinuity of PES around CI is common <sup>[19][20]</sup>. Higher level of theory like CASSCF/CASPT2 needs to be employed to study this nonadiabatic photochemistry.

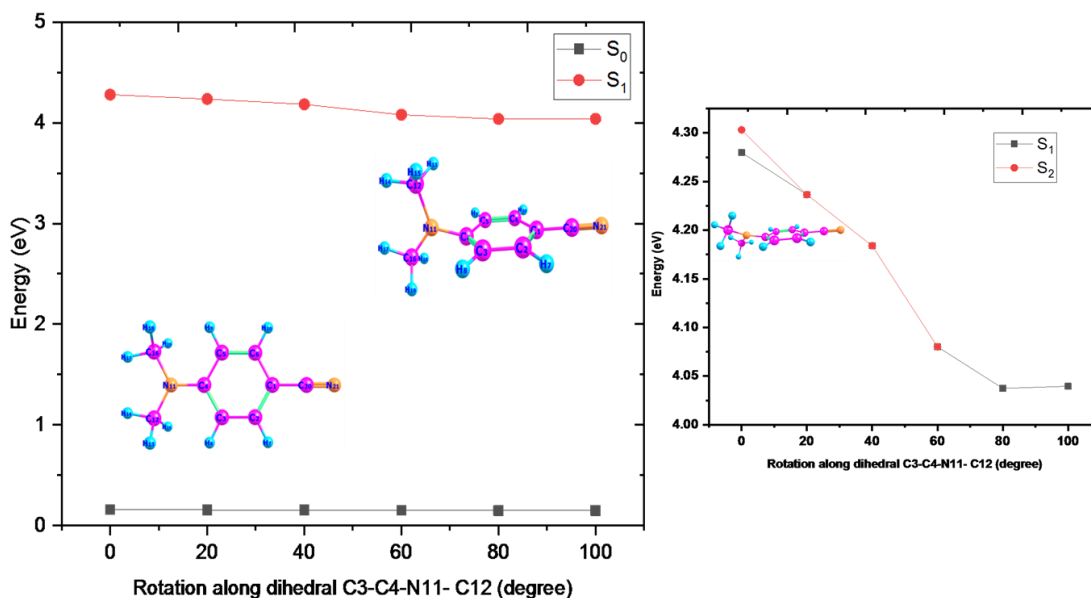


**Figure 4.4:** Constrained DFT/TDDFT optimization scans of the twist (rotation of  $C3-C4-N11-C12$  dihedral) on  $S_0$  and  $S_1$  excited state surfaces for DMABN in solvent phase (methanol) obtained at 6-31g+(d,p) basis set and wB97XD functional. The side figure shows  $S_1/S_2$  conical intersection that drives the TICT relaxation pathway.

### 4.3 TICT in DMPNA molecule

The correlation between charge separation in TICT state and “where the twist occurs” in the molecule (D-B-A) is also verified in the project. In case of DMABN, the dihedral rotation is in the single bond at the donor-spacer (D-B) end. N-dimethyl-p nitroaniline (DMPNA) is chosen to study how charge transfer in the excited state for TICT molecules follows twist in the molecular backbone. It shows how the nature of bond that rotates is not essentially similar coming to all TICT molecules. DMPNA has been a disputed example of TICT, where the thermodynamic feasibility of TICT formation has been realised by different groups including that of Dobkowski et al. Emission studies have shown weak fluorescence at lower temperatures, leading to many to dismiss possibility of a TICT state. However lack of TICT band could simply due to effective to intersystem crossing seen in nitro compounds <sup>[21]</sup>.

TD-DFT calculations from the  $S_0$  optimised coplanar geometry as well as pre-twisted –  $N(CH_3)_2$  on DMPNA shows a rotation of 73.5 degrees along the  $-NO_2$  bond (B-A) which is at the acceptor end following photoexcitation . This is different from DMABN and is verified with a MO analysis as shown in figure 4.4.

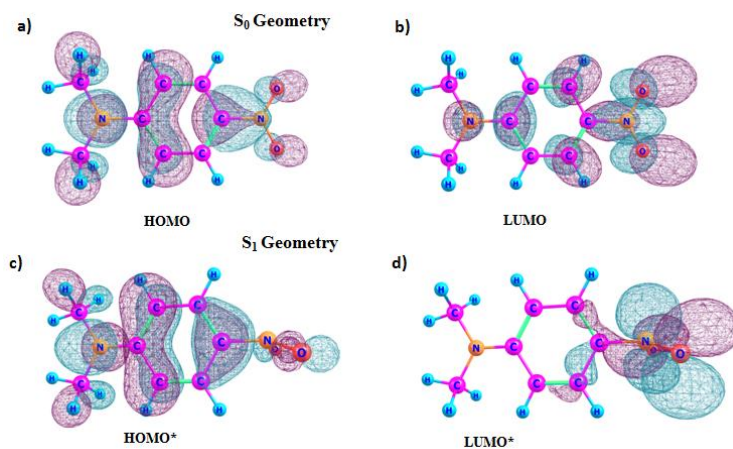


**Figure 4.5:** MO diagrams (isovalue 0.03) showing the flow of charge during vertical excitation and TICT a) HOMO b) LUMO of  $S_0$  planar geometry c) HOMO\* d) LUMO\* of  $S_1$  twisted geometry in DMPNA ,all obtained at 6-31g+(d,p) basis set and wB97XD functional in methanol solution IEFPCM model.



Several studies on the luminescence property of nitroaromatic molecules <sup>[22][23]</sup> show phosphorescence emission to be the major deactivation pathway of de-excitation in small ringed nitroaromatics. Stabilization of  $\pi$  MO's of the aromatic system relative to the n-MO situated on the nitro group and enhanced intramolecular charge-transfer character in a larger nitroaromatics results in nitro group acting as a mere spectator in emission characteristics.

## 4.4 TICT in DNS molecule

4-dimethylamino-4'-nitrostilbene (DNS) ground state geometry is optimised at M06-2X functional in DFT and 6-31g + (d,p) functional. The selection of functional is to include dispersive effects but at same instance, limit the calculation time which is higher in wB97XD. The M06-2X functionals do not contain an explicit dispersion term; but they have been parameterized to systems governed by dispersion interactions and are useful for modelling dispersion bound complexes <sup>[24]</sup>. The stilbene backbone of DNS is present in trans configuration with minimal steric hindrance along with dimethylamino donor group and nitro acceptor group. The calculation is performed with both explicit and implicit models. The explicit model contains methanol molecule (ratio 1:1 & ratio 1:2) that interact through space with the DNS molecule. While implicit solvation is done using IEFPCM model (methanol dielectric)(see Figure 4.6).

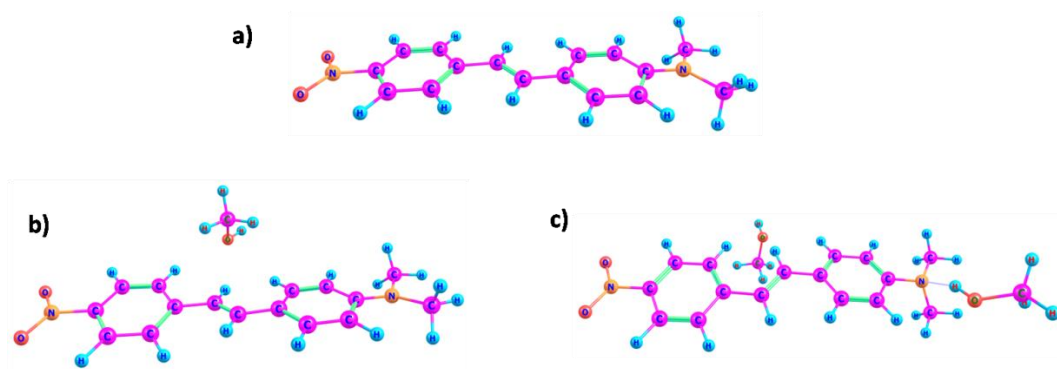


**Figure 4.6:** Ground state geometry of DNS optimized at M06-2X functional and 6-31g+(d,p) basis set using a ) IEFPCM solvation model for a methanol solvent b)Explicit solvation (ratio1:1) c) Explicit solvation (ratio1:2).

The ground state Raman active vibrational modes for DNS in both of the solvation models appear to be similar; however there appears to be additional dominant modes present in the explicit model (see Figure 4.7). This is due to fact that selection of MO6-2X functional is able to encapsulate Van der Waals interaction along with the other vibrations (see Figure 4.8).

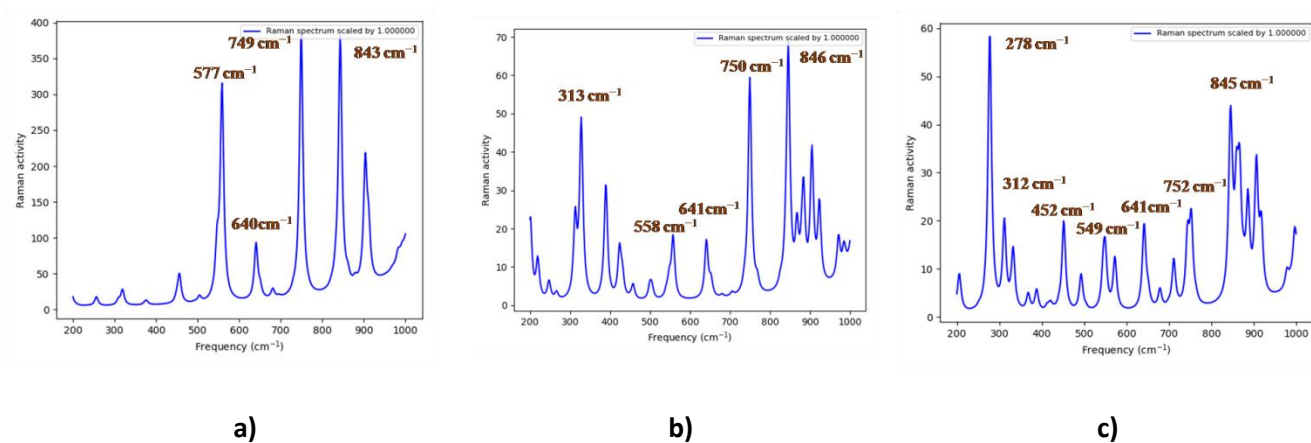


**Figure 4.7:** Simulated Raman active ground state vibrational modes obtained at a implicit solvation model b) explicit solvation model in 1:1 ratio c) explicit solvation model in 1:2 ratio of DNS and methanol obtained at 6-31g+(d,p) basis set and MO6-2X functional (unscaled).

The influence of van der Waals interaction on the vibrational mode can be traced through intense 278  $\text{cm}^{-1}$  in the 1:2 (DNS: methanol) model Vs 1:1 explicit model. Van der Waals radii are taken from Bondi's compilation <sup>[25]</sup> and the overlap of the spheres of influence can be seen as an analogy to the weak interaction. Implicit solvation model is used for further calculations to avoid contamination of methanol van der Waals interaction on the DNS molecular vibrations in case of explicit solvation.

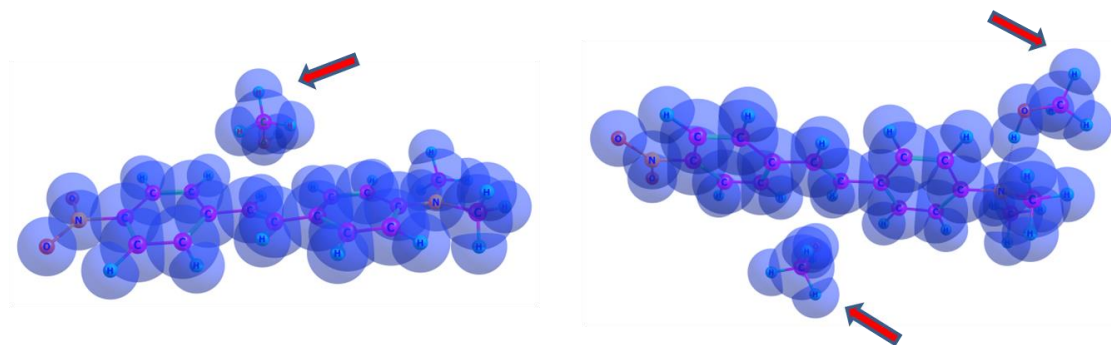


**Figure 4.8:** Van der Waals spheres in ground state obtained at a) explicit solvation model in 1:1 ratio b) explicit solvation model in 1:2 ratio of DNS and methanol using 6-31g+(d,p) basis set and MO6-2X functional. [Red arrow indicates position of methanol solvent molecule]

In DNS, excited state dynamics is particularly interesting as the twist in the excited state is around the stilbene backbone, realised in a number of studies [26]. In DNS, the twist along nitro group is not directly involved in electronic transition and relaxes via non radiative pathway <sup>[27]</sup>. The nature of the fluorescent relaxation along the isomerising dihedral is what makes DNS interesting molecule to look at. The parent stilbene shows two different isomers, a cis and a more thermodynamically stable trans form. The proposed pathway of the molecule is through a  $S_1/S_0$  conical intersection, relaxing into equilibrium ratio of cis/trans configurations depending upon the barrier of relaxation. Now when a donor and acceptor moiety is substituted into the complex along a covalent backbone, charge transfer can happen in the excited state (see Figure 4.9). The prospect of this TICT being coupled with isomerisation is yet to be completely explored.

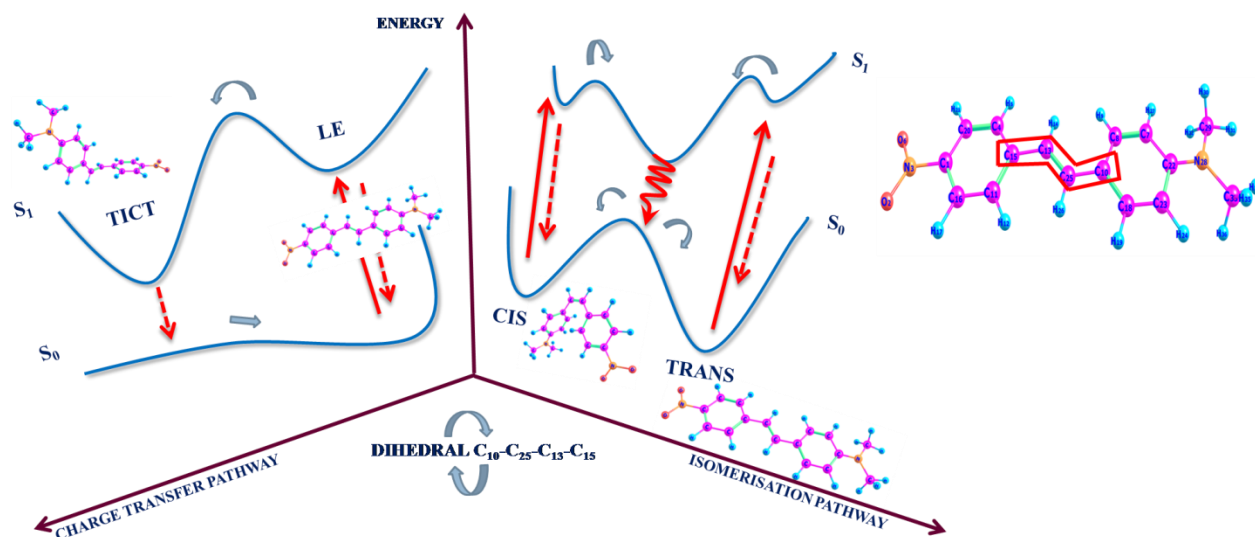


**Figure 4.9:** 2-D PES of DNS with projection along  $C_{10}-C_{25}-C_{13}-C_{15}$  dihedral coordinate represented in orthogonal planes, indicating the isomerisation pathway and charge transfer pathway.

Analysis of vibrational modes involved in the coupling serves as ideal tool to learn about the relaxation along ground and excited PES. Raman snapshot of DNS can be captured using ISRS and TR-ISRS experiments, which is characterised with DFT calculations.

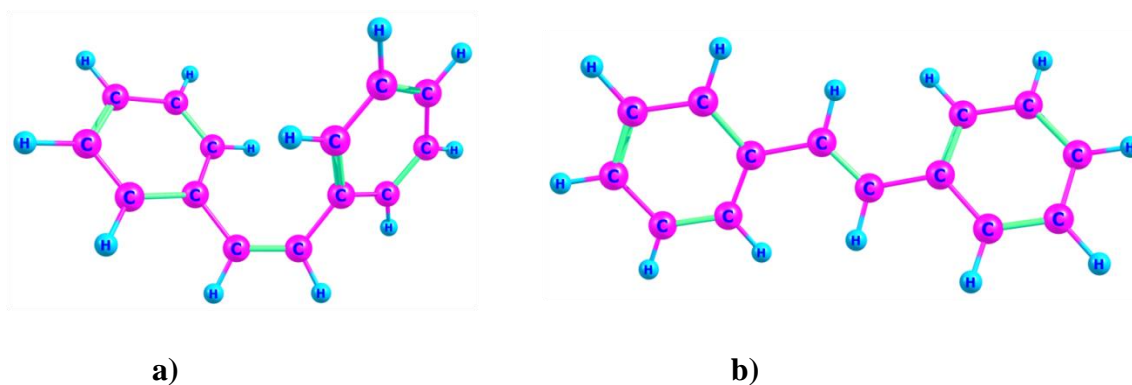


**Figure 4.10:** Optimised ground state geometry of a) cis-stilbene b) trans-stilbene obtained at 6-31g+(d,p) basis set and MO6-2X functional in methanol dielectric.

Trans and cis stilbene isomerisation in ground state calculations shows the involvement of dominant; ring breathing mode, a double bond twisting mode and benzene H in-plane-/ out-of-plane antisymmetric bending mode (see Figure 4.10). While the double bond twisting mode intensity remains almost the same, while the ring breathing mode seems to become stronger following cis to trans twist. The third mode which is a bending mode seems to be prominent in the cis geometry which could be dictating the steric hindrance following the two benzene rings coming closer to each other. The twist can hence be looked up in terms of linear combination of these modes with coefficient of the ring breathing mode being a marker for structural change during isomerisation.

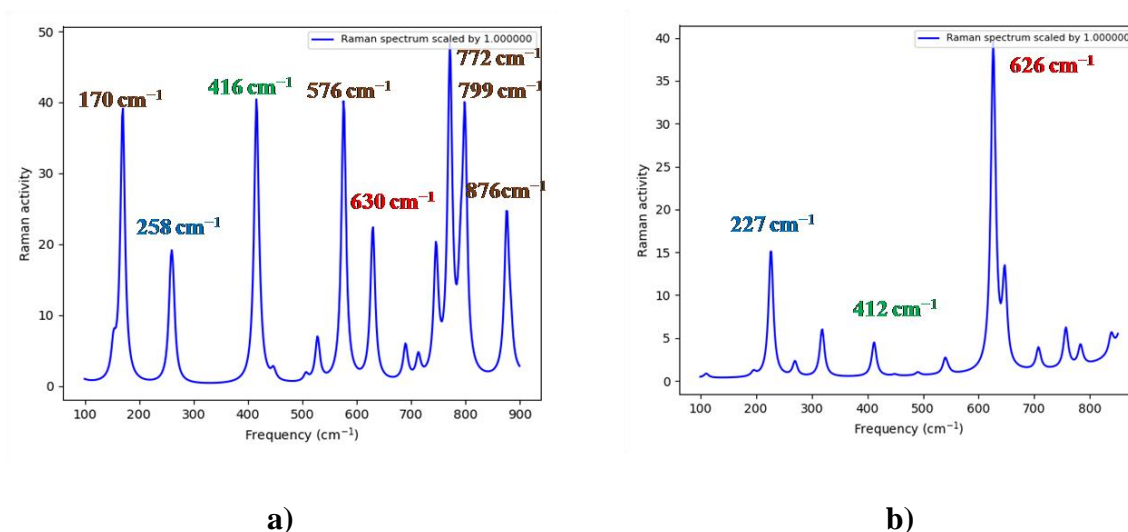


**Figure 4.11:** Simulated Raman active ground state vibrational modes obtained at a implicit solvation model b) of a) cis-stilbene b) trans-stilbene in methanol obtained at 6-31g+(d,p) basis set and MO6-2X functional [Red-Ring breathing mode, Blue-Double bond twisting mode, Green- Benzene H in-plane/-out-of-plane Antisymmetric Bending mode] (unscaled) .

In case of DNS, characterization of Raman activity spectrum (see Figure 4.7) indicates the same stilbene parent ring breathing mode at 640 cm<sup>-1</sup>. Apart from this, other dominant modes in the trans geometry at 558 cm<sup>-1</sup>, 749 cm<sup>-1</sup> and 843 cm<sup>-1</sup> are ring breathing modes involving donor-spacer-acceptor, donor-spacer and spacer-acceptor respectively. The involvement of

ring breathing modes involving the donor-acceptor moieties in ground and excited states of DMABN has been discussed in previous sections.

Time resolved impulsive stimulated Raman spectroscopy can now be employed to track the shift in frequencies and change in intensity of isomerisation and charge transfer modes, ultimately figuring out extent of coupling between these pathways.

## Conclusion

In summary, Impulsive Stimulated Raman Spectroscopy has proved to be a great technique to analyse molecular dynamics in chemical systems. Nile blue and methylene blue, ground as well as excited state vibrational modes have been identified using both experiment and theory. While Nile blue experiments were performed in a resonant fashion, methylene blue experiments were done in a slightly non-resonant manner. This change in photophysics in excitation for the two polyatomic molecules helps to understand how ground and excited vibrational coherence (VC) evolve. DFT and TD-DFT calculations helped to characterise the experimental vibrational modes and hence separate the Raman contributions from ground and excited VC respectively.

DMABN and DMPNA calculations give a clear picture on TICT in terms of the twist in structural backbone and associated HOMO-LUMO interaction that drives the formation of charge transfer state. In DMABN, the possibility of involvement higher electronic states and nonradioactive pathway like conical intersections leading to TICT fluorescence was realised. DMPNA on the other hand, shows that the charge transfer and relative localisation of molecular cloud in excited state can take place with twist along acceptor bond as well and is not necessarily along the donor bond as in DMABN.

DNS is interesting in terms of the excited state dynamics, as there exist a possibility of coupling between isomerisation and charge transfer pathways, both driving an excited to ground population transfer. The following could be realised using TR-ISRS and ISRS experiments and the vibrational modes that are involved in these structural dynamics be figured using DFT calculations.

# Bibliography

1. R. G Zbigniew, R Krystyna, S Aleksander , Dual fluorescence of donor-acceptor molecules and the Twisted Intramolecular Charge Transfer (TICT) states, J. Lumin, , **1979**
2. S Shunsuke, P. C. D Gregor, K Genichi, Recent advances in twisted intramolecular charge transfer (TICT) fluorescence and related phenomena in materials chemistry J. Mater. Chem. C, **2016**,4, 2731-2743
3. K. Rotkiewicz, K.H. Grellmann, Z.R. Grabowski, Reinterpretation of the anomalous fluorescence of p-n,n-dimethylamino-benzonitrile, Chem. Phys. Lett, **1973**
4. M.A. Haidekker, T.P. Brady, D. Lichlyter, E.A. Theodorakis, Effects of solvent polarity and solvent viscosity on the fluorescent properties of molecular rotors and related probes, Bioorg. Chem, Volume 33, Issue 6, **2005**, Pages 415-425
5. Z. R. Grabowski , K. Rotkiewicz and W. Rettig , Structural Changes Accompanying Intramolecular Electron Transfer: Focus on Twisted Intramolecular Charge-Transfer States and Structures ,Chem. Rev , **2003**, 103 , 3899 —4032
6. Mark G. Kuzyk; Manfred Eich; Robert A., Norwood, Linear and Nonlinear Optics of Organic Materials, **2010**, pp. 777408–777410.
7. Z.E. X. Dance, S. M. Mickley, T. M. Wilson, A. B. Ricks, A. M. Scott, M. A. Ratner, M. R. Wasielewski, Intersystem Crossing Mediated by Photoinduced Intramolecular Charge Transfer: Julolidine–Anthracene Molecules with Perpendicular  $\pi$  Systems, J. Phys. Chem. A, **2008**, 112, 18, 4194–4201
8. Zhou, F., Shao, J., Yang, Y., Zhao, J., Guo, H., Li, X., Ji, S. and Zhang, Z., Molecular Rotors as Fluorescent Viscosity Sensors: Molecular Design, Polarity Sensitivity, Dipole Moments Changes, Screening Solvents, and Deactivation Channel of the Excited States, Eur. J. Org. Chem, **2011**: 4773-4787.
- 9.: Bin Chen, Yubin Ding, Xin Li, Weihong Zhu, Jonathan P. Hill, Katsuhiko Arigac and Y. Xie , Steric hindrance-enforced distortion as a general strategy for the design of fluorescence “turn-on” cyanide probes, Chem. Commun, **2013**, 49, 10136



10. J.Kim, T.Morozumi, H.Higra, H.Nakamura, **Anal. Sci.**, ,Substituted Position Effect on Twisted Intramolecular Charge Transfer of 1- and 2-Anthracene Aromatic Carboxamides as Chemosensors Based on Linear Polyether, **2009**, 25, 1319–1325
11. Mukamel, S.; Biggs, Comment on the Effective Temporal and Spectral Resolution of Impulsive Stimulated Raman Signals, *J. Chem. Phys.*, **2011**, 134, 161101
12. Dhar L, Rogers J A, Nelson K A, Time-resolved vibrational spectroscopy in the impulsive limit, *Chem Rev*, **1994**, 94 157-193
13. Hohenberg P, Kohn W, Inhomogeneous electron gas, *Phys Rev B*, **1964**, 136:B864
14. E. Runge and E. K. U. Gross, Density-Functional Theory for Time-Dependent Systems, *Phys. Rev. Lett.*, **1984**, 52, 997
- 15..M. Shaul, Principles of nonlinear optical spectroscopy, (Oxford University Press Inc., New York), **1995**
16. Chen Z, Li Y, He Z, Xu Y, Yu W , Theoretical investigations on charge transport properties of tetrabenzo[a,d,j,m]coronene derivatives using different density functional theory functionals (B3LYP, M06-2X, and wB97XD, *Journal of Chemical Research.*, **2019**;43(7-8):293-303.
17. S. I Druzhinin.; N. P Ernsting.; S. A Kovalenko.; L. W Lustres.; T. A Senyushkina.; K. A Zachariasse, Dynamics of Ultrafast Intramolecular Charge Transfer with 4-(Dimethylamino)Benzonitrile in Acetonitrile, *J.Phys.Chem.A* , **2006**, 110, 2955–296910
18. Fuß, Werner,Pushpa, Kumbil Kuttan, Rettig, Wolfgang,Schmid, Wolfram E, Trushin, Sergei A, Ultrafast charge transfer via a conical intersection in Dimethylaminobenzonitrile, *Photochem. Photobiol. Sci.*, **2002**,1, 255-262
19. S Gozem,.; F Melaccio,.; A Valentini,.; M Filatov,.; M HuixRotllant,.; N.; Ferre, Frutos,.; L. M Angeli, C.; A. I Krylov,.; A. A Granovsky,.; R Lindh,.; M. Olivucci, Shape of Multireference, Equation-of-Motion Coupled-Cluster, and Density Functional Theory Potential Energy Surfaces at a Conical Intersection, *J. Chem. Theory Comput* , **2014**, 10, 3074
20. B. G Levine ; Ko, C.; J Quenneville,.; T. J Martínez., Conical Intersections and Double Excitations in Time-Dependent Density Functional Theory, *Mol. Phys.*, **2006**, 104, 1039.
- 21..A Gall, A.A.Pascal, B. Robert, Vibrational techniques applied to photosynthesis:Resonance Raman and fluroscence line-narrowing,*Biochim. Biophys. Acta Bioenergy*, **2015**, 1847, 12-18

22. S. Khalil, H. G. Bach, and S. P. McGlynn, *J. Mol. Spectrosc.* 35, 455 (**1970**)
23. T. P. Carsey, G. L. Findley, and S. P. McGlynn, *J. Am. Chem. Soc.* 101,4502 (**1979**)
24. M. Walker, A. J. A. Harvey, A. Sen, C. E. H. Dessent, Performance of M06, M06-2X, and M06-HF Density Functionals for Conformationally Flexible Anionic Clusters: M06 Functionals Perform Better than B3LYP for a Model System with Dispersion and Ionic Hydrogen-Bonding Interactions, *Phys. Chem. A*, **2013**, 117, 47, 12590–12600.
25. A. Bondi, Vander Waals Volumes and Radii, *J. Phys. Chem.*, **1964**, 68(3):441-451
26. J. Oberlé, E. Abraham, G. Jonusauskas and C. Rullière, Study of the intramolecular charge-transfer (ICT) process in 4-dimethylamino-4-nitrostilbene by picosecond time-resolved CARS, *J. Raman Spectrosc.*, **2000**, **31**, 311–317
27. H. K. Sinha and K. Yates. Ground- and excited-state dipole moments of some nitroaromatics: Evidence for extensive charge transfer in twisted nitrobenzene systems, *J. Chem. Phys.*, **1990**, 93, 7085